IEEE Access
Multidisciplinary : Rapid Review : Open Access Journal

Received March 23, 2020, accepted April 27, 2020, date of publication May 11, 2020, date of current version July 8, 2020.

Digital Object Identifier 10.1109/ACCESS.2020.2993762

Optimal Power Flow Solution With an Embedded Center-Node Unified Power Flow Controller Using an Adaptive Grasshopper Optimization Algorithm

AYMAN ALHEJJI [1], MOHAMED EBEED HUSSEIN [2], SALAH KAMEL [3], AND SAEED ALYAMI [4]

[1]Department of Electrical and Electronics Engineering Technology, Yanbu Industrial College, Yanbu 41912, Saudi Arabia
[2]Department of Electrical Engineering, Faculty of Engineering, Sohag University, Sohag 82524, Egypt
[3]Department of Electrical Engineering, Faculty of Engineering, Aswan University, Aswan 81542, Egypt
[4]Department of Electrical Engineering, College of Engineering, Majmaah University, Al-Majmaah 11952, Saudi Arabia

Corresponding author: Ayman Alhejji (alhejjia@rcyci.edu.sa)

ABSTRACT This paper proposes an adaptive grasshopper optimization algorithm (AGOA) for solving the optimal power flow (OPF) problem with the optimal incorporation of a center-node unified power flow controller (C-UPFC). The C-UPFC which is an advanced flexible AC transmission system (FACTS) device is inserted in series with a transmission line (TL) at its midpoint for providing the power flow control together with independent voltage control. The proposed AGOA is based on applying the Levy flight distribution and spiral path orientation of search agents to the traditional grasshopper optimization algorithm (GOA) to diminish the stagnation problem of the basic GOA at local optima and enhance its searching ability. Therefore, this AGOA technique is implemented for optimal sizing and siting of the C-UPFC on standard IEEE 30-bus and 57-bus systems as well as 26-bus system, and then compared with other well-known techniques to verify its effectiveness. To assess the installation of the C-UPFC in a power system, the optimal capacities and locations of the C-UPFC are determined for different objective functions, such as the fuel cost, fuel cost with a valve point loading effect (VPLE), piecewise cost and emission. Simulation results reveal that the proposed algorithm is more efficient and superior for OPF solution compared with the other algorithms reported in the literature. Furthermore, the optimal integration of the C-UPFC in the power system is considerably minimizing the power loss and improving the voltage profile.

INDEX TERMS Optimal power flow, C-UPFC, adaptive grasshopper optimization algorithm, fuel cost, emission.

I. INTRODUCTION

A. PROBLEM DEFINITION

The optimal power flow (OPF) problem is considered one of the most important problems in electric power systems. Dommel and Tinney [1] first discussed and formulated the OPF problem. The OPF problem solution refers to assigning the most adequate points, including generator output power, generator voltage, transformer tap, compensator output VAr, and FACTS parameters, to minimize the predefined objective functions while satisfying the operating system constraints. The considered objective functions include the fuel cost, power loss, harmful emissions due to thermal unit operation and enhancement of the voltage profile loadability and stability. Generally, flexible AC transmission systems (FACTSs) are typically connected to power systems to change the system parameters to enhance the performance and stability of electrical systems. The two main types of FACTS are categorized based on their power electronic components: variable impedance types, such as static VAr compensators (SVCs), thyristor-controlled phase shifting transformers (TCPSTs) and thyristor-controlled series capacitors (TCSCs), and voltage source converter (VSC)–based types, such as generalized power flow controllers (GUPFC)s, interline power flow controllers (IPFCs), static synchronous compensators (STATCOMs), static unified power flow controllers (UPFCs) and synchronous series compensators (SSSCs). It is worth mentioning that modeling VSC-based FACTS controllers in load flow algorithms requires more effort compared to variable impedance-based FACTS because complex modifications are required to incorporate their control parameters in the load flow algorithm, which leads to a loss of

The associate editor coordinating the review of this manuscript and approving it for publication was Shichao Liu.

Jacobian symmetry, admittance, and power mismatch matrices. Therefore, modeling these FACTSs is not an easy task [2], [3]. A C-UPFC is an effective FACTS device that is inserted in series with a transmission line (TL) at its midpoint to control the voltage at this point, the active power in the TL, the sending side reactive power flow and the receiving side reactive power flow in the TL [4]–[8]. There are few studies that examine C-UPFC modeling, and there are no papers that assess the optimal allocation of C-UPFCs in power systems. It should be pointed out that the reason for selection of the C-UPFC instead of the UPFC is that the C-UPFC is superior compared to the UPFC in terms of the control ability where the C-UPFC consists of three voltage source converters (VSCs) capable of providing complex control and adjusting four power system parameters including the voltage magnitude of the midpoint of the TL, the active power flow in this line and the reactive power at sending and receiving sides of the TL while the UPFC consists of VSCs can adjust only three parameters including the voltage magnitude of a certain bus as well as the active and reactive powers flow in the TL [6] and [72].

The GOA is a swarm-based technique that simulates the migration and grasshoppers in nature [9] and has been applied to solve several engineering problems [10]–[14]. It should be noted that the GOA is prone to local solutions in some cases. Therefore, many modifications have been made to the GOA technique to enhance its searching ability [15]–[18]. In this paper, the searching ability of the basic GOA is improved by applying the Levy flight distribution (LFD) to allow the algorithm to jump to new areas to avoid stagnation and enhance its exploration process, and the exploitation of the algorithm is enhanced by updating the positions of the grasshoppers in the spiral path with respect to the best solution.

B. BACKGROUND OUTLOOK

Many classic methods and meta-heuristic techniques have been employed to address the OPF problem. The classic methods include quadratic programming, Newton's method, linear programming, interior point and nonlinear programming [19]–[24]. The classic methods are prone to stagnation and may converge to local minima due to the highly nonlinear nature of OPF problems. Meta-heuristic algorithms have been widely applied to OPF problem solutions because they can offer notable performance compared with classic techniques; the main merits of meta-heuristic algorithms are as follows:

(1) High reliability to capture the optimal solutions.
(2) Applied systems are small and large.
(3) Rarely trapped in local minima.
(4) Exhibit good convergence characteristics.

Meta-heuristic techniques are categorized based on their inspiration concepts as follows:

(1) Swarm-based algorithms such as particle swarm optimization (PSO) [25], glowworm swarm optimization [26], artificial bee colony (ABC) [27], grasshopper optimization [28], and the grey wolf optimizer [29], [30]. Also, the modified shuffle frog leaping algorithm [31], moth-flame algorithm [32], flower pollination algorithm [33], and stud krill herd algorithm [34].

(2) Human-based algorithms such as teaching–learning-based optimization (TLBO) [35], improved harmony algorithm [36], Tabu search [37], imperialist competitive algorithm [38], and symbiotic organisms search algorithm [39].

(3) Evolutionary-based algorithms such as the differential evolutionary (DE) algorithm [40], genetic algorithm (GA) [41], evolutionary algorithm (EA) [42], improved genetic algorithm [43], etc.

(4) Physics-based algorithms such as colliding bodies optimization [44], gravitational search algorithm [45], [46], black hole-based optimization [47], simulated annealing [48], etc.

(5) Hybrid-based algorithms such as the fuzzy harmony search algorithm [49], artificial bee colony algorithm with quantum theory [50], particle swarm optimization and the shuffle frog leaping algorithm [51], etc. The authors in [52] produced an excellent survey for conventional and advanced metaheuristic optimization techniques that have been utilized for OPF solutions.

VSC-based FACTS devices have notable performance compared with variable impedance-based FACTS, as VSC-based FACTS can inject voltages with controllable magnitudes and controllable phase angles. Thus, these controllers can control the active and reactive power flows in a system separately or concurrently. Moreover, they have a fast response to any change in power systems. Several efforts have been made to optimally integrate VSC-based FACTSs in transmission systems for different objective functions, as depicted in Table 1.

C. CONTRIBUTION OF THIS WORK

The main aim of the presented work is an OPF solution using an AGOA that includes a C-UPFC. The contributions of this paper can be summarized as follows:

(1) The OPF problem is solved by incorporating a developed model of the C-UPFC, where the main merits of the proposed model are that the complex modifications of load flow are avoided by including a C-UPFC.
(2) A novel version of the GOA is presented for improving the exploration and exploitation phases of the basic GOA by implementing the Levy flight distribution along with adaptive spiral path orientation.
(3) The proposed algorithm is successfully implemented for the OPF problem and validated on a standard IEEE system.
(4) The optimal integration of the C-UPFC is assessed in terms of fuel cost, the fuel cost considering VPLE, piecewise cost and emission minimization.
(5) The optimal parameter settings and positions of the C-UPFC are successfully determined using the AGOA for the considered objective functions.

D. PAPER LAYOUT

The remaining sections in this paper are arranged as follows. Section 2 shows the modeling and operation principle of

TABLE 1. Summary regarding optimization techniques for optimal integration of VSC-based FACTSs.

Controller	Ref.	Algorithm	Objective functions
STATCOM	[53]	Particle Swarm Optimization	Voltage profile
	[54]	Imperialist Competitive Algorithm	System Oscillations
	[55]	Firefly Algorithm	Loadability
	[56]	Moth-Flame Algorithm	Power Losses & System Stability
	[57]	Lightning Attachment Procedure Optimization	Fuel Cost, Voltage profile & loading margin Stability
	[58]	Particle Swarm Optimization	Power Losses & Stability
	[59]	Particle Swarm Optimization	Transient Stability
SSSC	[60]	Gravitational Search Algorithm	Stability enhancement
	[61]	Particle Swarm Optimization	Loss minimization
	[62]	Moth-Flame Optimization Algorithm	System security
	[63]	Chemical Reaction Optimization	Power Losses
	[64]	Tabu Search Algorithm	Frequency oscillations
	[65]	Evolutionary Algorithm	Transient performance
UPFC	[66]	Differential Evolution Algorithm	Power system security
	[67]	Hybrid Immune Algorithm	The overall cost
	[68]	Genetic Algorithm	Fuel cost
	[69]	Gravitational Search Algorithm	Power Losses& Fuel cost
	[70]	Hybrid Chemical Reaction Optimization Algorithm	Power Losses & voltage deviation
	[71]	BAT search algorithm	Power Losses
	[72]	Lightning Attachment Procedure Optimization	Fuel cost & Emissions

the C-UPFC. Section 3 describes the problem formulation, including the considered objective functions and the operating constraints. Section 4 illustrates the basic GOA. Section 5 depicts the proposed AGOA. Section 6 provides the obtained results and a discussion. The conclusions of this paper are outlined in section 7.

II. C-UPFC MODELING AND OPERATING PRINCIPLE

A C-UPFC is a developed controller inserted in series with a TL to control four parameters, including the midpoint voltage magnitude (V_j), the active power flow in a TL (P^{sp}), the reactive power flow at the sending side of a TL (Q_s^{sp}) and the reactive power at the receiving side of a TL(Q_r^{sp}). The C-UPFC comprises three VSCs. The first converter is installed as a shunt at the midpoint of the TL, while the sending side converter and the receiving side converter are connected in series with the TL, as depicted in Fig. 1 [5]–[8]. These converters are connected to the system using three coupling transformers (*Tsh, Tr, Ts*), and the other sides of the VSCs share a common DC bus.

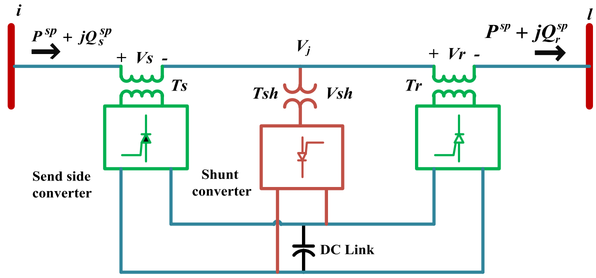

FIGURE 1. Structure of the C-UPFC.

The control strategy of the C-UPFC in steady state is similar to the other VSC -based controllers where the C-UPFC can control the power flow and the voltage magnitude by injecting AC voltages with controllable magnitudes and phase angles at center node.

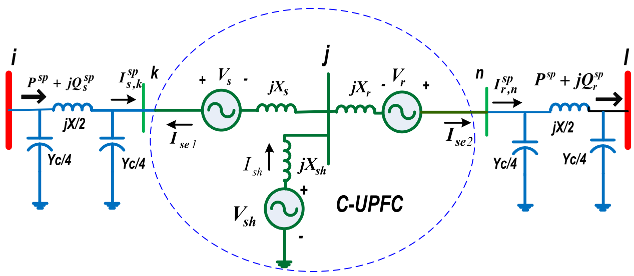

FIGURE 2. Voltage source model of C-UPFC.

The voltage source-based modeling of the C-UPFC is depicted in Fig. 2, where three voltage sources denote the C-UPFC representation. The C-UPFC terminals are represented by three buses (*k, j, n*) to determine the power flow through the controller. The midpoint bus (*j*) is represented as a PV bus, while the others (*k, n*) are represented as PQ buses. According to Fig. 2, the transmission line impedance and susceptance are divided. To model the series converters, the voltage source model of the series converter is converted to the current source model according to (1) and (2) as follows:

$$I_s = \frac{V_s}{jX_s} \tag{1}$$

$$I_r = \frac{V_r}{jX_r} \tag{2}$$

Then, these currents are converted to shunts, as depicted in Fig. 3, and calculated as a function of the specified values $(P^{sp}, Q_s^{sp}, Q_r^{sp}, V_j)$ by implementing the Kirchhoff current law at buses *(k, n)* as follows:

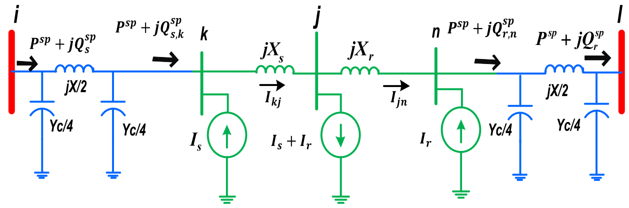

FIGURE 3. Shunt-injected current representations of series. converters.

KCL at bus k:

$$I_s = I_{kj} - I_{s,k}^{sp} = \frac{V_k - V_j}{jX_s} - \left(\frac{S_{s,k}^{sp}}{V_k}\right)^* \tag{3}$$

where

$$S_{s,k}^{sp} = P^{sp} + jQ_{s,k}^{sp} \tag{4}$$

$$I_{se1} = -I_{s,k}^{sp} = -\left(\frac{S_{s,k}^{sp}}{V_k}\right)^* \tag{5}$$

$$Q_{s,k}^{sp} = Q_s^{sp} + V_i^2\frac{B}{4} - I_{ik}^2\frac{X}{2} + V_k^2\frac{B}{4} \tag{6}$$

KCL at bus n:

$$I_r = I_{r,n}^{sp} - I_{jn} = \left(\frac{S_{r,n}^{sp}}{V_n}\right)^* - \frac{V_j - V_n}{jX_r} \tag{7}$$

where

$$I_{se2} = I_{r,n}^{sp} = \left(\frac{S_{r,n}^{sp}}{V_n}\right)^* \tag{8}$$

$$S_{r,n}^{sp} = P^{sp} + jQ_{r,n}^{sp} \tag{9}$$

$$Q_{r,n}^{sp} = Q_r^{sp} - V_l^2\frac{B}{4} + I_{nl}^2\frac{X}{2} - V_n^2\frac{B}{4} \tag{10}$$

The shunt currents are represented by complex loads as follows:

$$S_k = -V_k \times (I_s)^* \tag{11}$$

$$S_n = -V_n \times (I_r)^* \tag{12}$$

$$S_j = V_j \times (I_s + I_r)^* \tag{13}$$

The series-injected voltages can be determined using (11) and (12) by substituting the values of I_s and I_r from (1) and (2) into (3) and (7), respectively.

$$V_s = -\left(\frac{S_{s,k}^{sp}}{V_k}\right)^* \times jX_s + V_k - V_j \tag{14}$$

$$V_r = \left(\frac{S_{r,n}^{sp}}{V_n}\right)^* \times jX_r - V_j + V_n \tag{15}$$

From Fig. 2, the injected active powers from the sending and receiving converters (P_{ex1}, P_{ex2}) into the TL are found as follows:

$$P_{ex1} = Re\left(V_s\,(I_{se1})^*\right) \tag{16}$$

$$P_{ex2} = Re\left(V_r\,(I_{se2})^*\right) \tag{17}$$

In the C-UPFC, similar to a VSC-based FACTS in terms of the power flow in the controller, the net exchange of real power between the controller and the system equals zero if the converter losses are neglected. The shunt converter injects apparent power to the system ($P_{sh} + jQ_{sh}$). The main function of P_{sh} is to balance the power through the converters. Thus, P_{sh} is calculated using (18) as follows:

$$P_{sh} = -P_{ex1} - P_{ex2} \tag{18}$$

The injected complex loads at the midpoint node are given as follows:

$$P_j^{load} = P_j - P_{sh} \quad \text{and } Q_j^{load} = Q_j$$

where P_j denotes the real term of S_j, while Q_j denotes the imaginary part. The injection Q_{sh} by the shunt converter controls the magnitude of the midpoint voltage at the required value. Thus, the midpoint node is represented as a PV bus. The reactive power (Q_{sh}) can be founded using the balanced reactive power at the midpoint as described in (19).

$$Q_{sh} = V_jV_k\left(G_{kj}\sin\delta_{kj} - B_{kj}\cos\delta_{ij}\right) + V_jV_n\left(G_{nj}\sin\delta_{nj} - B_{nj}\cos\delta_{nj}\right) + Q_j^{load} \tag{19}$$

Referring to Fig. 1, the injected V_{sh} c and injected I_{sh} can be found using (17) and (18).

$$V_{sh} = V_j + jX_{sh}\left(\frac{P_{sh} + jQ_{sh}}{V_j}\right)^* \tag{20}$$

$$I_{sh} = I_{se1} + I_{se2} \tag{21}$$

Fig. 4 depicts the final proposed C-UPFC model, where the C-UPFC is represented by injected complex loads (S_k, S_n, P_j^{load}) and generated reactive power (Q_{sh}) at bus j. These loads are included in the power mismatch vector of the Newton-Raphson load flow method and updated as a function of P^{sp}, Q_s^{sp}, Q_r^{sp} and V_j.

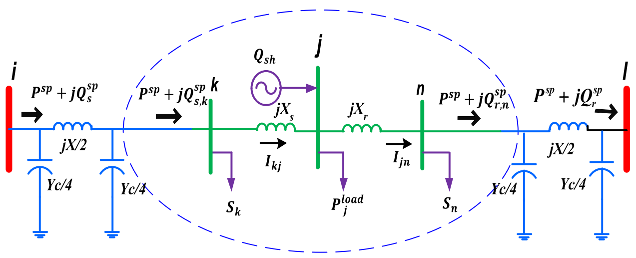

FIGURE 4. The developed power injection model of the C-UPFC.

III. PROBLEM FORMULATION

The OPF aims to assign the best operating point of power system control variables considering the predefined objective function while satisfying the system operating constraints. The optimal power flow is considered a nonlinear problem and is represented as follows [52]:

$$\text{Minmization } J(x, u) \tag{22}$$

$$\text{subject to } g_j(x, u) = 0 \quad j = 1, 2, \ldots, \tag{23}$$

$$h_i(x, u) \le 0 \quad i = 1, 2, \ldots, k \tag{24}$$

where J denotes the considered objective function, and u denotes the control variables x in the system, while denotes the dependent variables .g_j and h_j denote the equality and inequality system constraints, respectively. The control and dependent variables considering the C-UPFC variables are indicated in (25) and (26), respectively, as follows:

$$u = \begin{bmatrix} P_{G2}\ldots P_{G,NG}, V_{G1}\ldots V_{G,NG}, Q_{C1}\ldots Q_{C,NC}, T_1\ldots T_{NT}, \\ P^{sp}, Q_s^{sp}, Q_r^{sp}, V_j \end{bmatrix} \tag{25}$$

$$x = \begin{bmatrix} P_{G1}, V_{L,1}\ldots V_{L,NQ}, Q_{G1}\ldots Q_{G,NG}, S_{TL1}\ldots S_{TL,NTL}, \\ V_s, V_r, V_{sh} \end{bmatrix} \tag{26}$$

where
- P_G : The generation unit active power.
- V_G : The generation bus voltage.
- Q_C : The VAr output of the shunt compensator.
- T : The transformer tap setting.
- Q_G : The generation unit reactive power.
- V_L : The load bus voltage.
- S_{TL} : The apparent power flow in the TL.
- NQ : No. of load buses.
- NTL : No. of TLs.
- NG : No. of generators.
- NC : No. of compensator units.
- NT: No. of transformers.

A. OBJECTIVE FUNCTIONS

The considered objective functions in this paper are listed as follows:

1) FUEL COST MINIMIZATION

The first considered function is the total production fuel cost, which is described in (27).

$$J_1 = \sum_{i=1}^{NG} \left(a_i + b_i P_{Gi} + c_i P_{Gi}^2\right) \tag{27}$$

where a_i, b_i and c_i denote the cost coefficients.

2) FUEL COST FUNCTION MINIMIZATION WITH VPLE

The steam admission in generation units is subject to the continuous change in steam valves, which is known as the valve point loading effect (VPLE). The VPLE leads to fluctuations in the fuel cost, which can be considered by adding a sine term embedded in the fuel cost function [38], [39], [42], [81] and [82] as depicted in (28),

$$J_2 = \sum_{i=1}^{NG} \left(a_i + b_i P_{Gi} + c_i P_{Gi}^2\right) + \left| d_i sin(e_i(P_{Gi}^{min} - P_{Gi}))\right| \tag{28}$$

where d_i and e_i are the VPLE cost coefficients.

3) EMISSION MINIMIZATION

The third objective function is emission minimization, which is described using (29) as follows:

$$J_3 = Emission = \sum_{i=1}^{NG} \omega_i P_{Gi}^2 + \sigma_i P_{Gi} + \alpha_i + \zeta_i e^{(\lambda_i P_{Gi})} \tag{29}$$

where ω_i, σ_i, α_i, λ_i and ζ_i denote the emission coefficients.

4) PIECEWISE COST FUNCTION MINIMIZATION

The fourth considered function is the piecewise cost function. That cost is related to thermal generation, which consists of numerous fuel resources, including coal, oil and natural gas. Therefore, the cost function is represented as the collection of different cost functions for different fuel types as follows:

$$J_4 = F(P_{Gi}) = \begin{cases} a_{i1} + b_{i1} P_{Gi} + c_{i1} P_{Gi}^2 & P_{Gi}^{min} \le P_{Gi} \le P_{G1} \\ a_{i2} + b_i P_{Gi2} + c_i P_{Gi}^2 & P_{G1} \le P_{Gi} \le P_{G2} \\ \ldots \\ a_{ik} + b_i P_{Gik} + c_i P_{Gi}^2 & P_{Gi(k-1)} \le P_{Gi} \le P_{Gi}^{max} \end{cases} \tag{30}$$

B. CONSTRAINTS

1) EQUALITY CONSTRAINTS

$$P_{Gi} - P_{Di} = |V_i| \sum_{j=1}^{NB} |V_j| \left(G_{ij} cos\ delta_{ij} + B_{ij} sin\delta_{ij}\right) \tag{31}$$

$$Q_{Gi} - Q_{Di} = |V_i| \sum_{j=1}^{NB} |V_j| \left(G_{ij} cos\delta_{ij} + B_{ij} sin\delta_{ij}\right) \tag{32}$$

where P_{Di} denotes the active load demand, while Q_{Di} denotes the reactive load demand. B_{ij} and G_{ij} denote the susceptance and conductance of TL, respectively.

2) INEQUALITY CONSTRAINTS

$$\begin{cases} P_{Gn}^{min} \le P_{Gn} \le P_{Gn}^{\max} & n = 1, 2, \ldots, NG \\ V_{Gn}^{min} \le V_{Gn} \le V_{Gn}^{max} & n = 1, 2, \ldots, NG \\ Q_{Gn}^{min} \le Q_{Gn} \le Q_{Gn}^{max} & n = 1, 2, \ldots, NG \\ T_n^{min} \le T_n \le T_n^{max} & n = 1, 2, \ldots, NT \\ Q_{Cn}^{min} \le Q_{Cn} \le Q_{Cn}^{max} & n = 1, 2, \ldots, NC \\ S_{Ln} \le S_{Ln}^{max} & n = 1, 2, \ldots, NTL \\ V_{Ln}^{min} \le V_{Ln} \le V_{Ln}^{max} & n = 1, 2, \ldots, NQ \\ V_S^{min} \le V_s \le V_S^{\max} \\ V_r^{min} \le V_r \le V_r^{\max} \\ V_{sh}^{min} \le V_{sh} \le V_{sh}^{\max} \end{cases} \tag{33}$$

where the min and max superscripts are the allowable lower and upper limits of the control variables, respectively. The dependent variables are considered in the optimization problem as well as there are three constraints related to the C-UPFC which are the series injected voltages (V_s, V_r) and the shunt injected voltage (V_{sh}) are considered into the objective functions follows:

$$\begin{aligned} J_g(x,u) = {} & J_i(x,u) + \omega_G\left(P_{G1}-P_{G1}^{lim}\right)^2 \\ & + \omega_Q\sum_{n=1}^{NG}\left(Q_{Gn}-Q_{Gn}^{lim}\right)^2 + \omega_V\sum_{n=1}^{NQ}\left(V_{Ln}-V_{Ln}^{lim}\right)^2 \\ & + \omega_S\sum_{n=1}^{NTL}\left(S_{Ln}-S_{Ln}^{max}\right)^2 + \omega_{Vs}\left(V_s-V_s^{\lim}\right)^2 \\ & + \omega_{Vr}\left(V_r-V_r^{\lim}\right)^2 + \omega_{Vsh}\left(V_{sh}-V_{sh}^{\lim}\right)^2 \end{aligned} \tag{34}$$

where ω_G, ω_Q, ω_V, ω_S, ω_{Vs}, ω_{Vr} and ω_{Vsh} are the penalty factors.

$$\begin{cases} If\ P_{G1} > P_{G1}^{max} & then\ P_{G1}^{lim} = P_{G1}^{max} \\ elseIf\ P_{G1} < P_{G1}^{min} & then\ P_{G1}^{lim} = P_{G1}^{min} \end{cases} \tag{35}$$

$$\begin{cases} If\ Q_{Gn} > Q_{Gn}^{max} & then\ Q_{Gn}^{lim} = Q_{Gn}^{max} \\ elseIf\ Q_{Gn} < Q_{Gn}^{min} & then\ Q_{Gn}^{lim} = Q_{Gn}^{min} \end{cases} \tag{36}$$

$$\begin{cases} If\ V_{Ln} > V_{Gn}^{max} & then\ V_{Ln}^{lim} = V_{Gn}^{max} \\ elseIf\ V_{Ln} < V_{Gn}^{min} & then\ V_{Ln}^{lim} = V_{Gn}^{min} \end{cases} \tag{37}$$

$$\begin{cases} If\ V_s > V_S^{\max} & then\ V_s^{\lim} = V_S^{\max} \\ elseIf\ V_s < V_{Gn}^{min} & then\ V_s^{\lim} = V_{Gn}^{min} \end{cases} \tag{38}$$

$$\begin{cases} If\ V_r > V_r^{\lim} & then\ V_r^{lim} = V_r^{\max} \\ elseIf\ V_r < V_r^{\lim} & then\ V_r^{lim} = V_r^{min} \end{cases} \tag{39}$$

$$\begin{cases} If\ V_{sh} > V_{sh}^{\max} & then\ V_{sh}^{lim} = V_{sh}^{\max} \\ elseIf\ V_{sh} < V_{sh}^{min} & then\ V_{sh}^{lim} = V_{sh}^{min} \end{cases} \tag{40}$$

IV. OVERVIEW OF GOA

The GOA is an innovative algorithm that mimics the migration and interaction of grasshoppers in real life, where the adult grasshoppers travel in large swarms over a far distance, which simulates the exploration process of the algorithm, and the nymphs travel over a small distance, which simulates the exploitation process. The swarms are collected together when a large group of individuals interact. The orientation of the swarm depends on environmental factors, including wind speed, air temperature and sunshine. It is well known that grasshopper swarms move in a rolling motion when downwind, where the insects in the front of the swarm go down to the ground to eat and rest and then start to fly again. Fig. 5 shows the movement of the grasshoppers along with the wind. The grasshopper swarming action is based on downwind advection—the interaction between the insects and gravity. Therefore, the mathematical representation of the swarm behavior is represented as follows [9]:

$$X_k = m_1\gamma_k + m_2\beta_k + m_3\varphi_k \tag{41}$$

where X_k represents the grasshopper location. m_1, m_2 and m_3 denote random numbers within [0,1]. γ_k, β_k and φ_k are the social collaborations between the grasshopper and the gravity force on the k-th grasshopper.

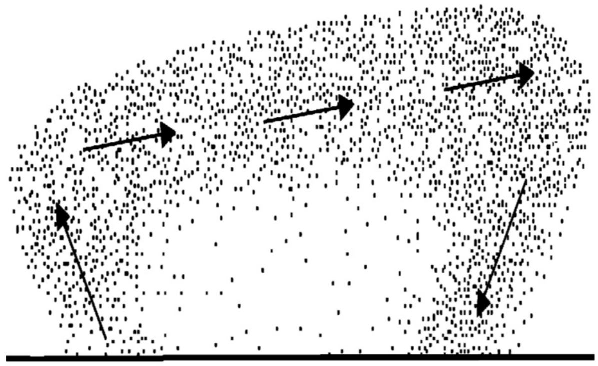

FIGURE 5. Movement of grasshoppers along with wind.

The collaboration between grasshoppers is represented as follows:

$$\gamma_k = \sum_{\substack{j=1 \\ k\neq j}}^{N} s\left(D_{kj}\right)\left(\frac{x_k - x_j}{D_{kj}}\right) \tag{42}$$

where

$$D_{kj} = \left|x_k - x_j\right|$$
$$s\left(D_{kj}\right) = Ae^{\frac{D_{kj}}{h}} - e^{D_{kj}} \tag{43}$$

where A denotes the attractive force. h denotes the attractive length. The gravity forces lead to a direct effect on the grasshopper swarm, which can be represented as follows:

$$\beta_k = -g\overrightarrow{e_g} \tag{44}$$

where g denotes a gravitational constant. $\overrightarrow{e_g}$ represents a unit vector toward the center of the earth. The third factor that affects swarm behavior is wind motion, which can be formulated as follows:

$$\varphi_k = u\overrightarrow{e_w} \tag{45}$$

where u is a constant. e_w is a unit vector based on the wind direction. Substituting the values of γ_k, β_k and φ_k from (42), (44) and (45) into (41) gives the following equation:

$$X_k = \sum_{\substack{j=1 \\ i\neq j}}^{N} s\left(D_{kj}\right)\left(\frac{x_k - x_j}{D_{kj}}\right) - g\overrightarrow{e_g} + u\overrightarrow{e_w} \tag{46}$$

where N denotes the number of grasshoppers. Herein, applying eq. (46) is unfitted to directly solve optimization problems because the grasshoppers quickly come to comfort zone, but the swarm does not move towards a specific point. Therefore, the modified transition of subsequent eq. (47) suggested by Saremi *et al.* [9] can predict the subsequent position of a grasshopper according to several potential positions such as current position, target position and all other grasshoppers' position as follows:

$$X_k = C\left(\sum_{\substack{j=1 \\ k\neq j}}^{N} C\left(\frac{U_k - L_k}{2}\right)s\left(D_{kj}\right)\left(\frac{x_k - x_j}{D_{kj}}\right)\right) + X_{best} \tag{47}$$

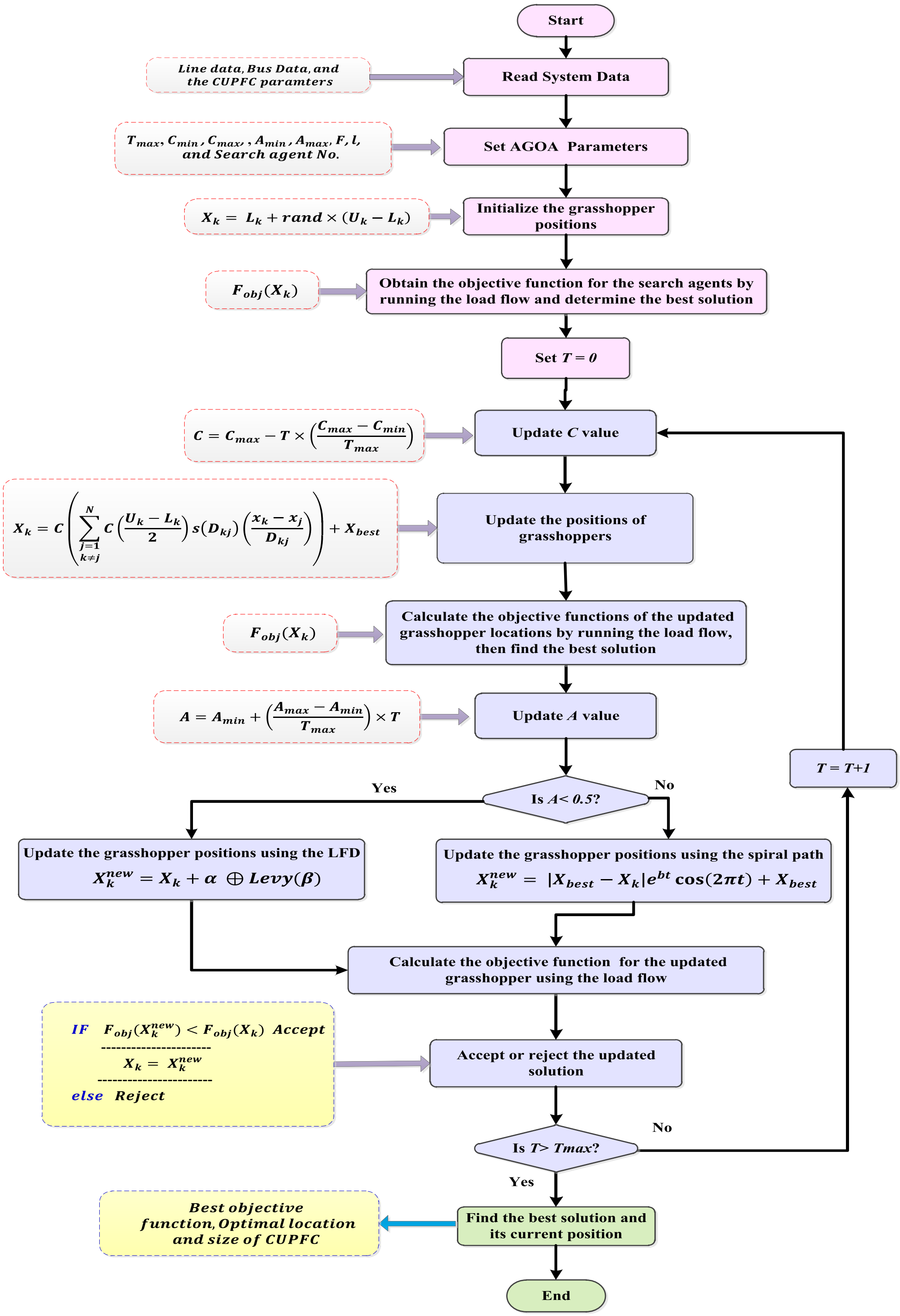

FIGURE 6. Procedure of the AGOA for solving OPF problem with allocation of the C-UPFC.

where U_k denotes the upper limit of the control variables, while L_k denotes the lower limit. X_{best} represents the best location. C denotes a linearly changed coefficient, which is calculated as follows:

$$C = C_{max} - T\left(\frac{C_{max} - C_{min}}{T_{max}}\right) \tag{48}$$

TABLE 2. The selected parameters of the AGOA.

Parameters	Value
T_{max}	100
Search agent No.	30
C_{max}	1
C_{min}	0.0004
F	0.5
L	1.5
A_{max}	0.85
A_{min}	0.45

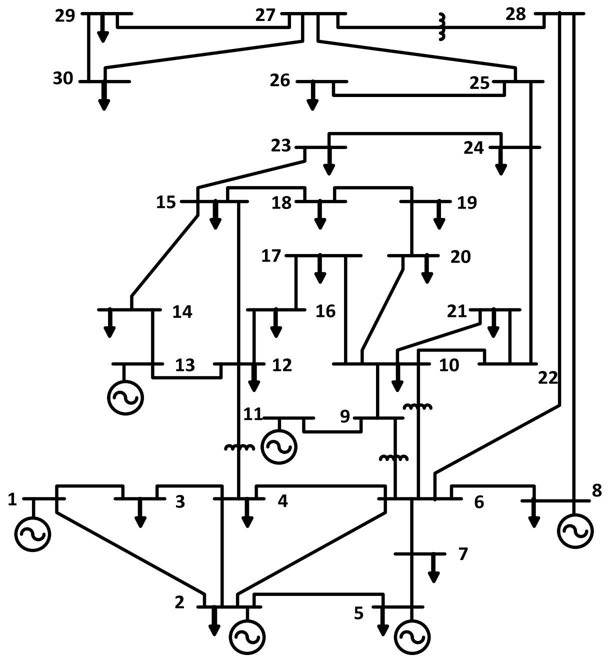

FIGURE 7. IEEE 30 bus system.

where C_{max} is the maximum limit of C, while C_{min} denotes the minimum limit. T represents the current iteration, and T_{max} denotes the maximum number of iterations.

V. OVERVIEW OF AGOA

The AGOA depends upon improving the exploitation and exploration processes of the basic GOA technique. The exploration phase of the basic GOA is enhanced using the Levy flight distribution (LFD) to allow the algorithm to jump to new positions to overcome GOA stagnation, while improving the exploitation of technique is based on updating the positions of the grasshoppers in a spiral path along with the best captured location. It is well-known that Levy flight denotes a random process to find novel solutions and depends upon a random walk. Its procedures are captured from the LFD. The novel location based on LFD can be obtained using (49):

$$X_k^{new} = X_k + \propto \oplus Levy\left(\beta\right) \tag{49}$$

where $\propto$ denotes a random step parameter. $\oplus$ denotes the entry-wise multiplication. β is a parameter related to the LFD.

TABLE 3. Cost coefficients of generation units.

Bus	P_G^{max} (MW)	P_G^{min} (MW)	a	b	c	d	e
1	200	50	0	2.0	0.00375	18	0.037
2	80	20	0	1.75	0.0175	16	0.038
5	50	15	0	1.0	0.0625	14	0.04
8	35	10	0	3.25	0.00834	12	0.045
11	30	10	0	3.00	0.025	13	0.042
13	40	12	0	3.00	0.025	13.5	0.041

TABLE 4. Emission coefficients of generation units.

Bus	α	σ	ω	ζ	λ
1	4.091	−5.554	6.49	2.00E-04	2.857
2	2.543	−6.047	5.638	5.00E-04	3.333
5	4.258	−5.094	4.586	1.00E-06	8
8	5.326	−3.55	3.38	2.00E-03	2
11	4.258	−5.094	4.586	1.00E-06	8
13	6.131	−5.555	5.151	1.00E-05	6.667

TABLE 5. Piecewise cost coefficients of generation units.

Bus	Power limit (MW)		Cost coefficients		
	Min.	Max.	a	b	c
1	50	140	55.0	0.70	0.0050
	140	200	82.5	1.05	0.0075
2	20	55	40.0	0.30	0.0100
	55	80	80.0	0.60	0.0200

The step size is given as:

$$\propto \oplus Levy\left(\beta\right) \sim 0.01 \frac{u}{|v|^{1/\beta}}\left(X_i^t - X_{best}^t\right) \tag{50}$$

where u and v denote variables obtained by normal distribution as :

$$u \sim N\left(0, \phi_u^2\right), \quad v \sim N\left(0, \phi_v^2\right) \tag{51}$$

$$\phi_u = \left[\frac{\Gamma\left(1+\beta\right) \times sin\left(\pi \times \beta/2\right)}{\Gamma\left[\left(1+\beta\right)/2\right] \times \beta}\right]^{1/\beta}, \quad \phi_v = 1 \tag{52}$$

where Γ represents the standard gamma function; $0 \leq \beta \leq 2$; for improving the exploitation of the GOA, the grasshopper position is updated by a logarithmic spiral function as depicted in (53).

$$X_k^{new} = |X_{best} - X_k|\, e^{bt} \cos\left(2\pi t\right) + X_{best} \tag{53}$$

where b is a constant used to define the logarithmic spiral shape. To balance the transposition between the exploration and exploitation processes, an adaptive parameter is utilized for this task, which can be given as follows:

$$A(T) = A_{min} + \left(\frac{A_{max} - A_{min}}{T_{max}}\right) \times T \tag{54}$$

where A_{max} and A_{min} denote the maximum and minimum limits of A. It should be noted that the value of the A parameter increases gradually with iteration progress when the value of A is small, as at the beginning of the iterative process. The grasshopper position is updated using LFD according to (49),

TABLE 6. Results of the OPF solution for different studied cases without including C-UPFC (IEEE 30-bus system).

Variables (p.u.)	Min.	Max.	Case 1 Fuel Cost		Case 2 Fuel Cost with VPLE		Case 3 Emission		Case 4 Piecewise Cost	
			AGOA	GOA	AGOA	GOA	AGOA	GOA	AGOA	GOA
P_{G1}	0.50	2.50	1.75768	1.75494	2.19816	1.93974	0.64077	0.64102	1.4	1.4
P_{G2}	0.20	0.80	0.48678	0.48457	0.28027	0.46363	0.6762	0.67841	0.55	0.54784
P_{G5}	0.15	0.50	0.21292	0.21391	0.15487	0.18795	0.5	0.5	24.406	24.382
P_{G8}	0.10	0.35	0.20698	0.21935	0.10	0.10028	0.35	0.35	0.34005	0.3459
P_{G11}	0.10	0.30	0.13736	0.13139	0.10	0.12842	0.3	0.3	0.18378	0.18991
P_{G13}	0.12	0.40	0.12	0.12	0.12	0.12000	0.4	0.4	0.18283	0.17466
V_1	0.95	1.1	1.0868	1.0707	1.089	1.0671	1.0474	1.039	1.0718	1.0551
V_2	0.95	1.1	1.0655	1.0547	1.0632	1.0442	1.0404	1.0224	1.0557	1.0418
V_5	0.95	1.1	1.0331	1.0263	1.0216	1.0067	1.0227	1.0715	1.0261	1.014
V_8	0.95	1.1	1.0398	1.0338	1.0292	1.0189	1.0327	1.0112	1.035	1.0211
V_{11}	0.95	1.1	1.0764	1.0442	1.0303	1.1	1.1	1.0021	1.0898	1.0595
V_{13}	0.95	1.1	1.0377	1.0084	1.0303	1.0549	1.0702	1.0585	1.0701	1.0083
T_{11}	0.9	1.1	0.99187	1.0963	1.0811	0.97097	0.99901	0.96673	1.053	1.0111
T_{13}	0.9	1.1	0.98616	1.0825	0.94223	1.0914	1.0806	0.90645	0.92232	0.98475
T_{15}	0.9	1.1	0.95596	1.0986	1.0124	1.0482	1.0147	0.9584	1.0075	0.99712
T_{36}	0.9	1.1	0.98354	1.0233	1.0105	1.0192	1.0263	1.0072	0.96751	1.0218
Q_{C10}	0	0.05	0.043112	0.027123	0.042337	0.017932	0.021164	0.039819	0.0042752	0.025382
Q_{C12}	0	0.05	0.040136	0.011816	0.032455	0.0	0.05	0.04463	0.024288	0.049993
Q_{C15}	0	0.05	0.045024	0.031861	0.029882	0.0	0.049698	0.01178	0.02868	0.042454
Q_{C17}	0	0.05	0.0015095	0.03485	0.044719	0.0	0.05	0.016549	0.02526	0.021508
Q_{C20}	0	0.05	0.0066628	0.05	0.019198	0.032939	0.0444	0.016545	0.029676	0.05
Q_{C21}	0	0.05	0.034307	0.0016004	0.040972	0.032631	0.047588	0.024651	0.006244	0.02297
Q_{C23}	0	0.05	0.013081	0.021017	0.004465	0.014727	0.05	0.049662	0.04729	0.027559
Q_{C24}	0	0.05	0.041318	0.039768	0.017044	0.0	0.043397	0.018781	0.046098	0.024466
Q_{C29}	0	0.05	0.032445	0.032786	0.035864	0.006259	0.05	0.05	0.003552	0.049833
Cost ($/h)			800.0212	800.9728	824.6063	836.2123	944.5704	945.5427	646.2795	647.3438
Emission(Ton/h)			0.3621	0.3614	0.3451	0.4196	0.20484	0.20492	0.2832	0.2833
VD (p.u)			0.7695	0.8874	0.8874	0.4574	0.6357	0.4340	0.7981	0.2902
P_{Loss} (MW)			8.7726	9.0149	11.9296	10.6027	3.3929	3.5482	6.6715	6.9247

VD: Summation of voltage deviations; P_{Loss}: power losses. Best objective function values are given in bold.

while at the final iterative steps of the iterative process, the grasshopper position is updated using a logarithmic spiral function according to (53) to improve the exploitation of the optimization technique. The AGOA implementation steps for solving the OPF with the C-UPFC are depicted in Fig. 6. It should be highlighted here that for calculating the parameters of the C-UPFC in this work, the specified values (P^{sp}, Q_s^{sp}, Q_r^{sp}, V_j) are defined by the optimization algorithm in each solution then the equations that describe the proposed power injection model of the C-UPFC are incorporated into Newton Raphson power flow. After convergence of the Newton Raphson method the parameters of the C-UPFC including V_s, V_r and V_{sh} are calculated according to (14), (15) and (20).

VI. SIMULATION RESULTS

The proposed algorithm is used for solving the OPF problem on the IEEE 30-bus, 26-bus and IEEE 57-bus test system to verify its validity. Moreover, the proposed algorithm is exploited to capture the optimal ratings and locations of the C-UPFC in the system to assess the optimal allocation of the C-UPFC in system performance with the considered objective functions. The proposed algorithm with the developed C-UPFC model was written using the MATLAB coding environment (MATLAB R2018b). The simulations were performed on a PC (Core I5, RAM 4.0 GB). The case studies are presented as follows:

A. IEEE 30-BUS TEST SYSTEM

The system load demand was 283.4 MW +j 126.2 MVAr. The IEEE 30 system consists of the following components:

- 6 generators at bus 1, bus 2, bus 5, bus 8, bus 11 and bus 13.
- 4 transformers branches at 6–9, 4–12, 6–10, and 27–28.
- 41 transmission lines.
- 9 capacitor banks at bus 10, bus 12, bus 15, bus 17, bus 20, bus 21, bus 23, bus 24 and bus 29.

The details of system data can be found in [73]. The system topology is depicted in Fig. 7. The voltage limit of the PV buses is [0.95, 1.1] p.u., while the PQ bus voltage limit is [0.95, 1.05] p.u. The transformer tap setting is set to [0.9, 1.1] p.u. The capacitor bank limit is set to [0.0, 5.0] MVAr. The allowable power flows in the transmission lines are listed in [75]. The allowable limit of injected series voltages of C-UPFC (V_s, V_r) is [0.001, 0.2] p.u., while the shunt voltage limit of C-UPFC is [0.9-1.1] p.u. The penalty factors of Eq. (34) are set to 1000. The selected parameters of the AGOA are tabulated in Table 2. The cost and emission coefficients of generators are depicted in Tables 3, 4 and 5.

TABLE 7. The obtained results of OPF solution for different studied cases including C-UPFC.

Variables (p.u)	Case 1 Fuel Cost		Case 2 Fuel Cost with VPE		Case 3 Emission		Case 4 Piecewise	
	AGOA	GOA	AGOA	GOA	AGOA	GOA	AGOA	GOA
P_{G1}	1.79945	1.78617	2.19813	2.18242	0.63711	0.64657	1.4	1.4
P_{G2}	0.47696	0.47094	0.24364	0.23807	0.67328	0.6741	0.55	0.54735
P_{G5}	0.21363	0.20822	0.15495	0.18042	0.5	0.5	22.554	22.542
P_{G8}	0.17655	0.1453	0.1	0.1	0.35	0.35	0.34045	0.34891
P_{G11}	0.11324	0.1733	0.1	0.10002	0.3	0.3	0.19086	0.18269
P_{G13}	0.12001	0.12	0.12	0.12	0.4	0.4	0.16913	0.17173
V_1	1.0535	1.039	1.0575	1.0428	1.0621	0.95	1.0745	1.057
V_2	1.041	1.0275	1.0449	1.0354	1.0544	0.9500	1.0572	1.0402
V_5	1.012 1	0.99626	1.0174	1.0419	1.0386	0.9601	1.0526	1.0311
V_8	1.0225	1.014	1.0272	1.042	1.0463	0.9814	1.0439	1.0307
V_{11}	1.0866	1.0228	1.0998	1.0197	1.0281	1.0606	1.0888	1.0556
V_{13}	1.0532	1.0692	1.0855	1.0763	1.0026	1.0644	1.0083	1.0765
T_{11}	1.0434	1.044	1.0086	1.1	0.95462	0.9000	1.0183	0.94648
T_{13}	0.90216	0.97652	0.95339	0.96721	1.1	1.0863	1.0807	1.0847
T_{15}	0.97855	1.0063	1.007	1.0829	1.0385	1.0718	0.98413	1.0463
T_{36}	0.95103	0.93612	0.95182	1.0277	0.97123	0.9284	0.98069	0.97965
Q_{C10}	0.019543	0.020582	0.016081	0.014535	0.017027	0.0025	0.041929	0.046933
Q_{C12}	0.041751	0.025143	0	0.015135	0.041137	0.0415	0.035209	0.0051361
Q_{C15}	0.0011015	0.029311	0.0165	0.0098181	0.049401	0.0014	0.013177	0.026165
Q_{C17}	0.019298	0.032317	0.012241	0	0.049995	0.0381	0.0077255	0.048522
Q_{C20}	0	0.027383	0	0.010552	0.012903	0.0500	0.031749	0.049763
Q_{C21}	0.0203	0.049929	0.015127	0.026666	0.05	0.0345	0.041556	0.036798
Q_{C23}	0	0	0	0.042512	0.047106	0.0001	0.049716	0.001924
Q_{C24}	0.0082125	0.0020032	0.010772	0.0066989	0.049999	0.0226	0.0079981	0.049963
Q_{C29}	0.016702	0.029547	0.015659	0.00045053	0.043512	0.0446	0.023056	0.024012
Cost ($/h)	791.222	794.0913	812.6948	815.5579	942.4640	945.1438	636.6191	637.2239
Emission (Ton/h)	0.374658	0.36952	0.535979	0.526958	0.20464	0.20468	0.284053	0.2841677
VD (p.u)	0.5949	0.2738	0.7306	0.6241	0.425923	0.3962	0.4148	0.5519
P_{Loss} (MW)	6.5820	6.9919	8.2721	8.6936	2.6392	3.6660	4.1982	4.2102

TABLE 8. Optimal setting and sizing of C-UPFC for different studied cases (IEEE 30-bus system).

	Case 1		Case 2		Case 3		Case 4	
	AGOA	GOA	AGOA	GOA	AGOA	GOA	AGOA	GOA
Location	(1-3)	(1-3)	(1-3)	(1-3)	(2-6)	(2-6)	(2-5)	(2-5)
$V^{sp}(p.u)$	1.0283	0.9806	1.063	1.006	1.054	0.98	1.0509	0.978
$P^{sp}(MW)$	111.54	106.66	117.29	115.61	54.89	63.23	94.356	92.219
$Q_s^{sp}(MVAR)$	-7.35	-1.72	-23.02	-10.01	28.99	-16.08	35.833	16.317
$Q_r^{sp}(MVAR)$	9.44	-20.18	-5.70	-17.95	32.78	-14.86	54.253	-16.246
$V_s(p.u)$	0.1999 $\angle$-79.79°	0.2000 $\angle$-73.0°	0.2000 $\angle$-80.36°	0.2000 $\angle$-74.78°	0.0934 $\angle$-100.41°	0.1332 $\angle$- 92.21°	0.1731 $\angle$-90.73°	0.1730 $\angle$-79.93°
$P_{ex1}(MW)$	2.8000	6.0868	- 0.1505	4.3749	1.9535	-2.3334	0.6327	5.5283
$V_r(p.u)$	0.2000 $\angle$78.87°	0.1920 $\angle$89.54°	0.1983 $\angle$95.92°	0.1915 $\angle$ 85.21°	0.1301 $\angle$43.83°	0.1366 $\angle$ 106.711°	0.1737 $\angle$87.14°	0.1713 $\angle$87.72°
$P_{ex2}(MW)$	-2.4528	-4.0348	1.5216	-4.5784	-2.0115	0.1754	-0.2665	-4.7083
$V_{sh}\ (p.u)$	0.9675 $\angle$-0.41°	0.9000 $\angle$-0.50°	1.0656 $\angle$-0.95°	0.9302 $\angle$ -1.15°	0.9380 $\angle$-0.14°	1.0263 $\angle$0.42°	1.0426 $\angle$0.25°	0.9000 $\angle$0.35°
$P_{ex3}(MW)$	- 0.3472	-2.0521	-1.3712	0.2035	0.0581	2.1579	-0.3662	-0.8200

CASE 1: FUEL COST MINIMIZATION

In this case, the proposed algorithm is applied to reduce the fuel cost of generation units according to (27) with and without incorporating the C-UPFC. The obtained results of implementing the AGOA and the traditional GOA for solving the OPF problem over 30 runs without and with the C-UPFC are listed in Table 6 and Table 7, respectively. The optimal locations and sizing of the C-UPFC are listed in Table 8. The obtained fuel cost with applying the AGOA is 800.0212 $/h, which is better than the fuel cost using the GOA (800.9728 $/h) by 0.1188 %. Table 9 shows a comparison of the fuel costs obtained by different techniques. As shown in Table 8, it is clear that the minimum fuel cost is obtained by the AGOA compared with the GA [76], ITS [77], EP [77], TS/SA [77], TS [77], IEP [17], MDE [78], TS [37], ABC [27], SOS [39], MSA [79], GWO [30], DGWO [30], MFO [32] and IMFO [32]. In the case of optimal integration of the C-UPFC, the fuel cost has been reduced from 800.0212 $/h to 791.222 $/h, i.e., the fuel cost is reduced by 8.7992 $/h (1.0998 %) with inclusion of the C-UPFC. In this case,

TABLE 9. Comparative results by AGOA and other optimization techniques for case 1.

Algorithm	Worst Cost	Average Cost	Best Cost	Time (s)	Method Description	REF.
GA	NA	NA	805.937	NA	Genetic Algorithm	[76]
ITS	806.856	805.812	804.556	88.495	Improved Tabu Search	[77]
EP	803.474	803.232	802.907	66.693	Evolutionary Programming	[77]
TS/SA	803.291	803.032	802.788	62.275	Hybrid Tabu Search and Simulated Annealing	[77]
TS	802.746	802.632	802.502	86.227	Tabu Search	[77]
IEP	802.581	802.521	802.465	99.013	Improved Harmony Evolutionary Programming	[77]
MDE	802.404	802.382	802.376	23.25	Modified Differential Evolution	[78]
TS	NA	NA	802.290	NA	Tabu Search	[37]
ABC	801.8674	800.8715	800.6600	NA	Artificial Bee Colony Algorithm	[27]
SOS	801.8821	801.7251	801.5733	60.1245	Symbiotic Organisms Search Algorithm	[39]
MSA	NA	NA	800.5099	14.91	Moth Swarm Algorithm	[79]
TLBO	801.0586	800.8661	800.4212	22.14	Teaching– Learning-Based Optimization	[80]
GWO	804.898	802.663	801.259	53.6	Grey Wolf Optimizer	[30]
DGWO	800.4989	800.4674	800.433	37.8	Developed Grey Wolf Optimizer	[30]
MFO	NR	NR	800.6206	NA	Moth Flame Optimizer	[32]
IMFO	NR	NR	800.3848	NA	Improved Moth Flame Optimizer	[32]
GOA	803.8165	802.3332	800.9728	34.33	Grasshopper Optimizer Algorithm	
AGOA	801.0658	800.35628	800.0212	37.61	Adaptive Grasshopper Optimizer Algorithm	

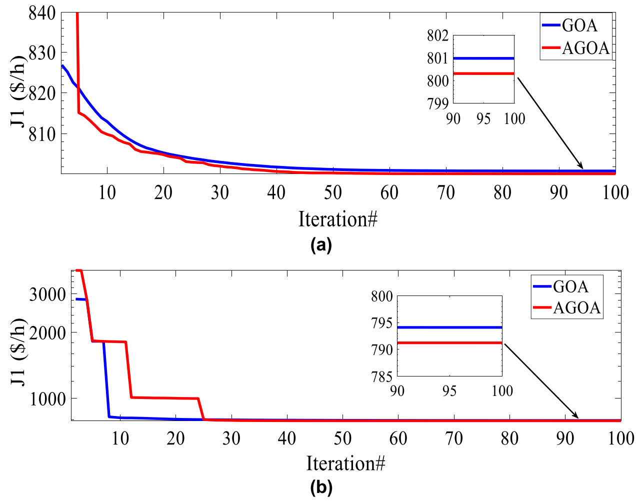

FIGURE 8. Convergence plot for case 1: (a) without C-UPFC; (b) with C-UPFC.

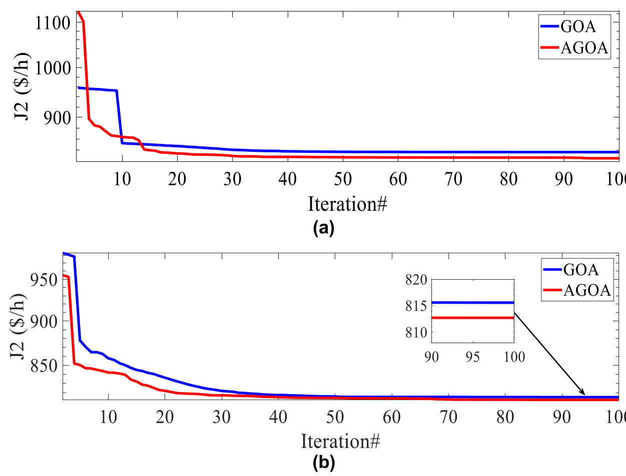

FIGURE 9. Convergence plot for case 2: (a) without C-UPFC; (b) with C-UPFC.

the optimal rating and location of the C-UPFC are tabulated in the 2nd and 3rd columns of Table 8. Fig. 8 shows the trends of the objective function. It is clear that the AGOA has stable and robust convergence characteristics.

CASE 2: FUEL COST MINIMIZATION WITH VPLE

The objective function for this case is reducing fuel cost by considering the VPLE, as described in (28). The optimal fuel costs for this case determined by the AGOA are 824.6063 $/h and 836.2123$/h; thus, the obtained cost by the AGOA is better than that obtained by the GOA. Table 10 shows the fuel cost obtained by the AGOA and other well-known optimization algorithms. Referring to Table 10, the cost obtained by the AGOA is better than the tabulated algorithms, including GA-MPC [83], SA [82], PSO [82], SFLA [82], SFLA-SA [82], BSA [81], SOS [39] and GWO [30]. In the case of optimal integration of the C-UPFC, the fuel cost has been reduced from 824.6063 $/h (without C-UPFC) to 812.6948 $/h, i.e., the fuel cost is reduced by 11.9115 $/h (1.444 %) with inclusion of the C-UPFC. The placement and size of the C-UPFC for this case are depicted in the 4th and 5th columns of Table 8. Fig. 9 illustrates the convergence plot of the considered objective function. It is notable that the AGOA converged quite smoothly to the best solution.

CASE 3: EMISSIONS MINIMIZATION

Reducing the emissions is the required objective function according to (29). The optimal assigned values of the control variables determined by the AGOA and GOA without a C-UPFC are depicted in the 8th and 9th columns of Table 6, while those with the C-UPFC are depicted in the 6th and 7th columns of Table 7. The emissions value obtained by the AGOA is 0.20484 ton/h, which is less than the emissions value obtained by the GOA (0.20492 ton/h). Table 11 depicts the optimal emission values assigned by

TABLE 10. Comparative results by AGOA and other optimization techniques for case 2.

Algorithm	Worst Cost	Average Cost	Best Cost	Time (s)	Method Description	REF.
GA-MPC	830.4928	830.4406	830.4379	NA	Genetic Algorithm with multi-parent crossover	[83]
SA	NA	NA	827.8262	119.48	Simulated Annealing	[82]
PSO	NA	NA	826.5897	24.75	Particle Swarm Optimization	[82]
SFLA	NA	NA	825.9906	22.83	Shuffle Frog Leaping Algorithm	[82]
SFLA-SA	NA	NA	825.6921	21.48	Shuffle Frog Leaping Algorithm and Simulated Annealing	[82]
BSA	830.15	827.69	825.23	NA	Backtracking Search Algorithm	[81]
SOS	825.5275	825.4039	825.2985	120.42	Symbiotic Organisms Search Algorithm	[39]
GWO	852.1109	844.4588	835.554	41.70	Grey Wolf Optimizer	[30]
GOA	844.0129	839.5368	836.2123	50.86	Grasshopper Optimizer Algorithm	
AGOA	825.4175	825.0135	824.6063	68.39	Adaptive Grasshopper Optimizer Algorithm	

TABLE 11. Comparative results by AGOA and other optimization techniques for case 3.

Algorithm	Worst	Average	Best	Time (s)	Method Description	REF.
SKH	0.2051	0.2049	0.2048	16.54	Stud Krill Herd Algorithm	[84]
KH	0.2054	0.2050	0.2049	18.02	Krill Herd Algorithm	[84]
ARCBBO	0.2064	0.2054	0.2048	NA	Adaptive Real Coded Biogeography-Based Optimization	[85]
ABC	NA	NA	0.204826	NA	Artificial Bee Colony	[27]
TLBO	NA	NA	0.205	NA	Teaching–Learning Based Optimization	[86]
MTLBO	NA	NA	0.20493	NA	Modified Teaching–Learning Based Optimization	[86]
GOA	0.2128	0.20709	0.20492	46.17	Grasshopper Optimizer Algorithm	
AGOA	0.20487	0.204854	0.20484	66.51	Adaptive Grasshopper Optimizer Algorithm	

TABLE 12. Comparative results by AGOA and other optimization techniques for case 4.

Algorithm	Worst cost	Average cost	Best cost	Time (s)	Method Description	REF.
ITS	675.035	664.473	654.874	94.832	Improved Tabu Search	[77]
TS/SA	662.616	658.234	654.378	73.243	Hybrid Tabu Search and Simulated Annealing	[77]
TS	658.911	654.087	651.246	88.447	Tabu Search	[77]
EP	657.120	654.501	650.206	69.865	Evolutionary Programming	[77]
ABC	659.7708	654.0784	649.0855	NA	Artificial Bee Colony Algorithm	[27]
MDE	650.664	648.356	647.846	37.05	Modified Differential Evolution	[32]
TLBO	647.8415	647.8335	647.8125	24.37	Teaching– Learning-Based Optimization	[80]
PSO	647.87	647.73	647.69	NA	Particle Swarm Optimization	[25]
LTLBO	647.8638	647.4725	647.4315	22.78	Lévy Teaching– Learning-Based Optimization	[80]
GSA	646.9381	646.8962	646.8480	10.2716	Gravitational Search Algorithm	[46]
GWO	648.681	647.432	646.426	47.2	Grey Wolf Optimizer	[30]
GOA	649.1766	648.5064	647.3438	31.79	Grasshopper Optimizer Algorithm	
AGOA	646.9915	646.6742	646.2795	50.00	Adaptive Grasshopper Optimizer Algorithm	

well-known algorithms. Judging from Table 11, the best obtained emission value can be obtained by implementing the AGOA compared with SKH [84], KH [84], ARCBBO [85], ABC [27], TLBO [86] and MTLBO [86]. In the case of optimal integration of the C-UPFC, the emissions have been minimized from 0.20484 ton/h (without C-UPFC) to 0.20464 ton/h using the AGOA, which verifies the effectiveness of optimal integration of the C-UPFC. The location and parameter settings of the C-UPFC using the AGOA and GOA for this case are depicted in the 6th and 7th columns of Table 8, respectively. Fig. 10 illustrates the convergence plot of the emissions values. The AGOA exhibits excellent convergence characteristics.

CASE 4: PIECEWISE FUEL COST MINIMIZATION

The piecewise fuel cost functions are the considered function depicted in (30). In this case, generator#1 and generator#2 are represented by piecewise cost functions [87]. The generator coefficients are listed in Table 5. The optimal costs obtained by implementation of the AGOA and GOA are 646.2795 \$/h and 647.3438 \$/h, respectively. From the presented comparison in Table 12, the obtained result by the AGOA is better than the obtained costs by the reported algorithms, including ITS [77], TS/SA [77], TS [77], EP [77], ABC [27], MDE [32], TLBO [80], PSO [25], LTLBO [80], GSA [46] and GWO [30]. In the case of optimal installation of the C-UPFC, the piecewise cost has been reduced from 646.2795 \$/h (without C-UPFC) to 636.6191 \$/h using the AGOA., i.e., the fuel cost is reduced by 9.6604 \$/h (1.49477 %) with inclusion of the C-UPFC, which verifies the effectiveness of optimal integration of the C-UPFC. The location and parameter settings of the C-UPFC using the AGOA and GOA for this case are shown in the 8th and 9th columns of Table 7, respectively. The convergence characteristic for

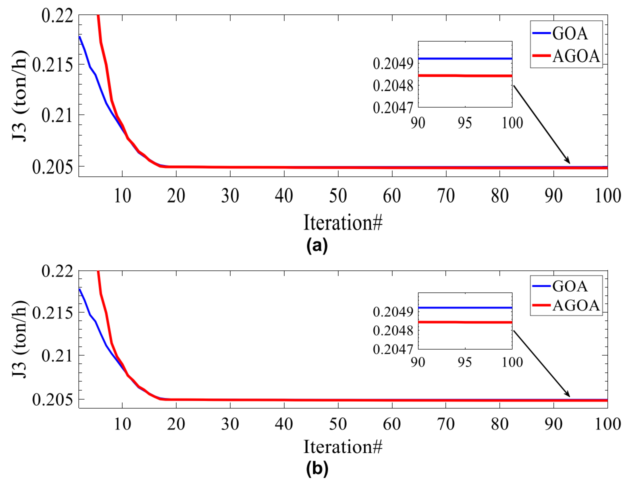

FIGURE 10. Convergence plot for case 3: (a) without C-UPFC; (b) with C-UPFC.

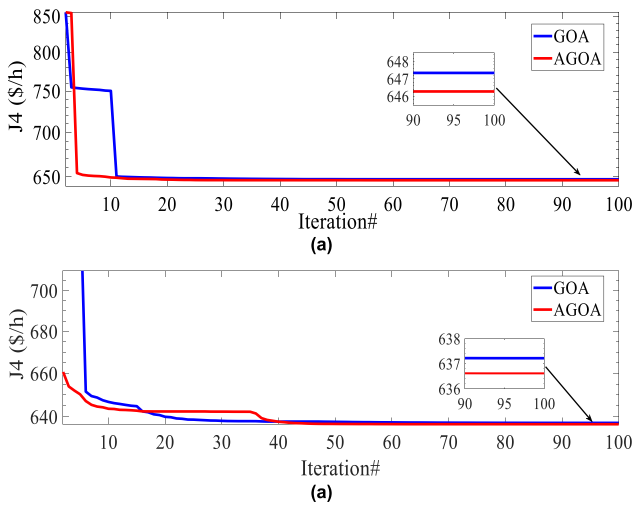

FIGURE 11. Convergence plot for case 4: (a) without C-UPFC; (b) with C-UPFC.

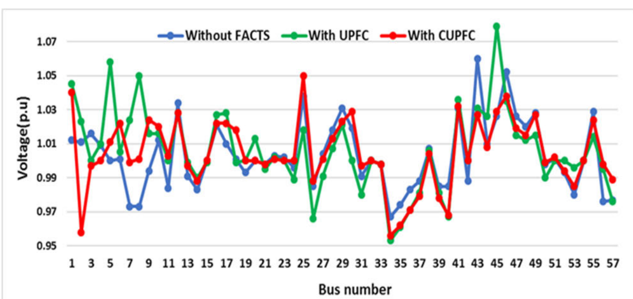

FIGURE 12. The voltage profile of IEEE 57-bus with UPFC and C-UPFC.

this case is depicted in Fig. 11. The proposed algorithm shows excellent convergence performance.

Referring to Tables 9, 10, 11, and 12, the simulation time of the AGOA is slightly more than GOA and some algorithms due to the additional steps for modifying of the traditional GOA but the obtained results by AGOA are better than those obtained by other reported techniques.

TABLE 13. Optimal setting and sizing of C-UPFC (26-bus system).

Parameters	AGOA	GOA
Location	(2-7)	(2-7)
$V^{sp}(p.u)$	1.032	0.976
$P^{sp}(MW)$	119.998	120.00
$Q_s^{sp}(MVAR)$	-7.37	-6.25
$Q_r^{sp}(MVAR)$	80.94	-24.63
$V_s(p.u)$	$0.1347 \angle -82.61^{o}$	$0.1472 \angle -69.92^{o}$
$P_{ex1}(MW)$	1.3647	5.4212
$V_r(p.u)$	$0.1655 \angle 52.93^{o}$	$0.1401 \angle 92.05^{o}$
$P_{ex2}(MW)$	-0.7000	-2.5079
$V_{sh}(p.u)$	$1.0010 \angle -1.13$	$0.9118 \angle -1.27^{o}$
$P_{ex3}(MW)$	-0.6647	-2.9133

B. 26-BUS TEST SYSTEM

The 26 system is the second test system which consists of the following components:

- 6 generators at bus 1, bus 2, bus 3, bus 4, bus 5 and bus 26.
- 7 transformers branches at 2–3, 2–13, 3–13, 4–8, 4–12, 6–19 and 7–19.
- 46 transmission lines.
- 9 capacitor banks at bus 1, bus 4, bus 5, bus 6, bus 9, bus 11, bus 12, bus 15 and bus 19.

The details of system data can be found in [88-89]. The considered objective function in this case is the quadratic fuel cost according to (27). The fuel cost obtained by applications of the GOA and the AGOA are 15448.409 $/h and 15432.817 $/h, respectively. This verified that the application of the AGOA for this case is better than GOA. The optimal locations and parameters setting of the C-UPFC are listed in Table 13 while the optimal settings of control values of this case are tabulated in Table 14. In case of incorporating C-UPFC optimally, the fuel cost is reduced to 15421.895 $/h and 15408.845 $/h using GOA and AGOA i.e., the fuel cost is reduced by 26.514 $/h (0.1716 %) and 23.972 $/h (16 %).

C. IEEE 57-BUS TEST SYSTEM

In this section, the C-UPFC is tested on IEEE 57-bus for minimizing the power losses and the voltage deviations as well as the obtained results are compared with those results obtained by optimal inclusion of the UPFC in system. The system load equals to 1250.8 MW + j 336.4 MVAR while the system data is given in [90]. The used model of the UPFC is simplified as depicted in [72]. The considered objective function in this section can be represented as follows:

$$\mathrm{VD} = \sum_{n=1}^{NB} |V_n - 1| \tag{55}$$

$$P_{loss} = \sum_{i=1}^{NTL} G_{ij}(V_i^2 + V_j^2 - 2V_iV_j cos\delta_{ij}) \tag{56}$$

TABLE 14. Results of the OPF solution with and without including C-UPFC (26-bus system).

Variables (p.u.)	Min.	Max.	Without C-UPFC		With C-UPFC	
			AGOA	GOA	AGOA	GOA
P_{G1}	1.00	5.00	4.4748	4.5257	4.4766	4.4774
P_{G2}	0.50	2.00	1.7198	1.8023	1.7249	1.6678
P_{G3}	0.80	3.00	2.6167	2.6507	2.6321	2.6599
P_{G4}	0.50	1.50	1.3184	1.1850	1.3468	1.2891
P_{G5}	0.50	2.00	1.7143	1.8278	1.7485	1.7063
P_{G26}	0.50	1.20	0.9038	0.7667	0.8005	.9388
V_1	0.95	1.1	1.0394	1.0258	1.0446	1.0225
V_2	0.95	1.1	1.0371	1.0277	1.0432	1.0211
V_3	0.95	1.1	1.0292	1.0183	1.0391	1.0221
V_4	0.95	1.1	1.0292	1.0343	1.0540	1.0194
V_5	0.95	1.1	1.0430	1.0338	1.0320	1.0210
V_{26}	0.95	1.1	1.0756	0.9839	0.9504	1.0150
T_{11}	0.9	1.1	1.0137	1.0664	1.0100	0.9594
T_{13}	0.9	1.1	0.9956	0.9171	1.0283	1.0384
T_{15}	0.9	1.1	0.9910	1.0077	0.9888	1.0042
T_{36}	0.9	1.1	1.0299	1.0419	1.0044	1.0118
T_{11}	0.9	1.1	1.0322	1.0392	1.0148	1.0350
T_{13}	0.9	1.1	0.9728	0.9425	0.9823	0.9817
T_{15}	0.9	1.1	0.9589	0.9719	0.9503	0.9574
Q_{C10}	0	0.05	0.0500	0.0398	0.0166	0.0448
Q_{C12}	0	0.05	0.0018	0.0426	0.0297	0.0339
Q_{C15}	0	0.05	0.0313	0.0157	0.0075	0.0433
Q_{C17}	0	0.05	0.0235	0.0442	0.0285	0.0042
Q_{C20}	0	0.05	0	0.0106	0.0017	0.0099
Q_{C21}	0	0.05	0.0275	0.0343	0.0457	0.0258
Q_{C23}	0	0.05	0.0265	0.0158	0.0474	0.0019
Q_{C24}	0	0.05	0.0288	0.0017	0.0430	0.0090
Q_{C29}	0	0.05	0.0088	0.0265	0.0402	0.0004
Cost ($/h)			15432.817	15448.409	15408.845	15421.895
P_{Loss} (MW)			11.776	12.866	9.9538	10.9247
VD (p.u)			0.2511	0.2430	0.4289	0.3240

TABLE 15. Optimal setting and sizing of C-UPFC (IEEE 57-bus system).

Parameters	VD	$Ploss$
Location	(3-4)	(1-15)
$V^{sp}(p.u)$	0.96748	1.03188
$P^{sp}(MW)$	61.917	79.577
$Q_s^{sp}(MVAR)$	13.803	79.2279
$Q_r^{sp}(MVAR)$	-0.32574	66.5195
$V_s(p.u)$	0.0155 $\angle$-39.87°	0.1246 $\angle$-131.26°
$P_{ex1}(MW)$	0.9453	1.3191
$V_r(p.u)$	0.0097 $\angle$110.62°	0.1413 $\angle$ 41.03°
$P_{ex2}(MW)$	0.0924	-2.3019
V_{sh} $(p.u)$	0.9173 $\angle$-12.45 °	0.9881 $\angle$-0.7802°
$P_{ex3}(MW)$	-1.0377	0.9828

TABLE 16. Optimal setting and sizing of UPFC (IEEE 57-bus system).

Parameters	VD	$Ploss$
Location	(5-6)	(21-22)
$V^{sp}(p.u)$	1.058	1.0140
$P^{sp}(MW)$	4.6401	-3.3511
$Q_s^{sp}(MVAR)$	-10.1102	14.6183
$V_{se}(p.u)$	0.1246 $\angle$116.025°	0.0474 $\angle$-71.07°
$P_s(MW)$	-0.0139	-0.0069
$V_{sh}(p.u)$	1.0759 $\angle$-7.10°	1.0229 $\angle$ -6.40°
$P_{sh}(MW)$	0.0139	0.0069

where, $\boldsymbol{VD}$ and $\boldsymbol{P_{loss}}$ are the summation of voltage deviations and system power losses in system, respectively.

The optimal setting of the C-UPFC and UPFC are listed in Table 15 and 16, respectively. Table 17 shows the optimal power flow solution of the IEEE 57-bus with inclusion the C-UPFC and the UPFC using the AGOA. Referring to Table 15 the system power loss without incorporating FACTS devices in system is 11.8112 MW while the power loss is reduced to 11.1153 MW and 10.7081 MW with optimal inclusion of the UPFC and C-UPFC, respectively which verifies the effectiveness of the C-UPFC compared with the UPFC.

The VD of system without incorporating FACTS devices in system is 0.7721 p.u. while the VD is alleviated to 0.7596 p.u.

TABLE 17. Results of the OPF solution with and without including C-UPFC (IEEE 57-bus system).

	Power losses			Voltage deviation		
Variable	Without FACTS	With UPFC	With CUPFC	Without FACTS	With UPFC	With CUPFC
PG1	1.1495		1.3858	3.2761	2.86082	
PG2	0.90716	0.598746	0.994158	0.23358	0.818996	0.4352
PG3	1.4	1.08788	1.32809	0.10649	0.0801003	0
PG6	0.59402	0.760688	0.726367	0.18992	0.880233	0.22947
PG8	3.5159	3.352	3.08067	4.733	3.88741	2.1818
PG9	0.95951	0.91511	0.99999	0.26541	0.74127	0.79981
PG12	4.1	4.09976	4.1	3.9152	3.43706	3.9995
VG1	1.0413	1.0631	1.06427	1.0123	1.04471	1.0397
VG2	1.0446	1.04094	1.05106	1.0112	1.02264	0.95776
VG3	1.0437	1.09991	1.06515	1.016	0.990038	0.9969
VG6	1.05	1.00241	1.04354	1.0009	0.954747	1.0219
VG8	1.0677	1.05216	1.04365	0.97294	1.08024	1.0011
VG9	1.0487	1.045	1.03686	0.99393	0.966179	1.0237
VG12	1.0435	1.04327	1.02761	1.0336	1.04832	1.0284
T19(4_18)	0.9451	1.07969	0.947325	1.0205	1.06786	0.98354
T20(4_18)	1.0401	1.04453	1.06875	0.99563	0.962346	0.96335
T31(21_20)	1.0376	0.981742	1.09026	0.97925	0.954402	1.0001
T35(24_25)	0.98774	0.966132	0.980701	0.93695	0.98857	0.91658
T36(24_25)	0.98291	1.0562	1.03384	0.98471	0.913964	1.0504
T37(24_26)	1.0457	1.04341	1.0197	1.0099	1.02429	1.0148
T41(7_29)	1.034	1.00888	0.989095	0.93675	1.0001	0.96672
T46(34_32)	1.042	0.921998	1.03351	0.93968	0.915447	0.94155
T54(11_41)	1.0664	0.907637	0.984446	0.91845	0.901304	0.90949
T58(15_45)	0.96113	0.987614	0.996301	0.97608	0.90529	0.97504
T59(14_46)	0.96724	0.983693	0.970651	0.91836	0.945783	0.94274
T65(10_51)	1.0076	1.00085	0.972235	1.0114	1.01319	1.0167
T66(13_49)	0.94278	0.956628	0.958034	0.90013	0.936805	0.90015
T71(11_43)	1.0029	1.06865	0.97024	0.91675	0.969334	0.97561
T73(40_56)	0.96922	1.00121	1.00384	1.069	0.905457	0.93083
T76(39_57)	0.99564	0.924802	1.006	0.94201	1.03574	0.97564
T80(9_55)	1.0739	1.00406	1.07089	0.95614	0.999482	0.99599
QC18	0.1697	0.113809	0.174357	0.093896	0.0681531	0.083852
QC25	0.16999	0.10726	0.184064	0.087841	0.0351662	0.14871
QC53	0.077571	0.110177	0.0754244	0.039291	0.197499	0.10688
VD	1.4356	1.0722	1.4790	0.7721	0.7596	0.7076
Lmax	0.2470	0.2266	0.2336	0.2621	0.2781	0.2487
Ploss (MW)	11.8112	11.1153	10.7081	21.3835	20.6441	39.9581

and 0.7076 p.u. with optimal inclusion of the UPFC and C-UPFC, respectively which verifies that the C-UPFC is more efficient for voltage profile improvement compared with the UPFC. The voltage profile for IEEE 57-bus with the C-UPFC and the UPFC is depicted in Fig. 12.

VII. OUTCOMES AND UNIQUE FEATURES

The unique features of this paper can be summarized as follows:

(1) Proposing a new Adaptive Grasshopper Optimization Algorithm (AGOA) for solving the stagnation problem of the traditional GOA based on Levy flight distribution and spiral path orientation.

(2) Application of the proposed AGOA can solve the optimal power problem efficiently compared with the basic GOA and other well-known published algorithms in terms of the objective functions where notable results are obtained and it can be depicted as:

-The fuel cost is reduced to 800.0212 ($/h) which is the best among the listed techniques in Table 9.

-Fuel Cost with VPE is reduced to 824.6063 ($/h) which is the best among the listed techniques in Table 10.

-Emission is reduced to 0.20484 (Ton/h) which is the best among the listed techniques in Table 11.

-Piecewise cost is reduced to 646.2795 ($/h) which is the best among the listed techniques in Table 12.

(3) Assigning the optimal location and size of the C-UPFC in power system is one of the main features presented in this paper where the location and size of the C-UPFC have not been presented so far.

(4) An optimal integration of the C-UPFC can reduce the fuel cost, the fuel cost with VPE, emission and piecewise cost considerably to 791.222 ($/h), 812.6948 ($/h), 0.20464 (Ton/h) and 636.6191 ($/h), respectively.

(5) The minimum fuel cost that obtained by incorporating the C-UPFC is 791.222 ($/h) which is better than the cost was obtained by optimal inclusion of UPFC (798.0251 ($/h)) [72].

(6) A comparison between the C-UPFC and the UPFC in terms of power loss and voltage profile improvement was carried out to verify the superiority of the C-UPFC.

VIII. CONCLUSION

This paper proposed an AGOA for solving the OPF problem with the optimal incorporation of a C-UPFC. The proposed algorithm was based on applying Levy flight distribution and spiral path orientation of search agents to the traditional grasshopper optimization algorithm to diminish the stagnation problem of the basic GOA and enhance its searching ability. The AGOA technique has been implemented on a standard IEEE 30-bus, 26-bus and IEEE 57-bus systems, and it has been compared with other well-known techniques to verify its effectiveness. The optimal capacities and locations of the C-UPFC have been determined for different objective functions to assess the installation of the C-UPFC in a power system. The results revealed that the proposed algorithm was a superior and more effective technique compared with the reported algorithms for solving the OPF problem. Moreover, encouraging results have been obtained with the optimal integration of a C-UPFC, where the fuel cost has been reduced from 800.0212 \$/h (without C-UPFC) to 791.222 \$/h. Additionally, the fuel cost with the VPLE has been reduced from 824.6063 \$/h to 812.6948 \$/h, the emissions have been reduced from 0.20484 ton/h to 0.20464 ton/h, and the piecewise fuel cost has been considerably reduced from 646.2795 \$/h to 636.6191 \$/h. Furthermore, the optimal integration of the C-UPFC minimized the power loss and improved the system voltage profile efficiently compared with the UPFC. In the future, multiple C-UPFCs can be optimally incorporated considering the uncertainties in a power system.

REFERENCES

[1] H. W. Dommel and W. F. Tinney, "Optimal power flow solutions," *IEEE Trans. Power App. Syst.*, vol. PAS-87, no. 10, pp. 1866–1876, Oct. 1968.

[2] K. Padiyar, *FACTS Controllers in Power Transmission and Distribution*. New Delhi, India: New Age International, 2007.

[3] Y.-H. Song and A. Johns, *Flexible ac transmission systems (FACTS)*. Edison, NJ, USA: IET, 1999.

[4] B. T. Ooi, M. Kazerani, R. Marceau, Z. Wolanski, F. D. Galiana, D. McGillis, and G. Joos, "Mid-point siting of FACTS devices in transmission lines," *IEEE Trans. Power Del.*, vol. 12, no. 4, pp. 1717–1722, Oct. 1997.

[5] B. T. Ooi and B. Lu, "C-UPFC: A new FACTS controller with 4 degrees of freedom," in *Proc. IEEE 31st Annu. Power Electron. Spec. Conf. (PESC)*, Jun. 2000, pp. 961–966.

[6] A. Ajami, S. H. Hosseini, S. Khanmohammadi, and G. B. Gharehpetian, "Modeling and control of C-UPFC for power system transient studies," *Simul. Model. Pract. Theory*, vol. 14, no. 5, pp. 564–576, Jul. 2006.

[7] S. Kamel, F. Jurado, and R. Mihalic, "Advanced modeling of center-node unified power flow controller in NR load flow algorithm," *Electr. Power Syst. Res.*, vol. 121, pp. 176–182, Apr. 2015.

[8] S. Kamel, M. Ebeed, J. Yu, and W. Li, "A comprehensive model of C-UPFC with innovative constraint enforcement techniques in load flow analysis," *Int. J. Electr. Power Energy Syst.*, vol. 101, pp. 289–300, Oct. 2018.

[9] S. Saremi, S. Mirjalili, and A. Lewis, "Grasshopper optimisation algorithm: Theory and application," *Adv. Eng. Softw.*, vol. 105, pp. 30–47, Mar. 2017.

[10] A. A. El-Fergany, "Electrical characterisation of proton exchange membrane fuel cells stack using grasshopper optimiser," *IET Renew. Power Gener.*, vol. 12, no. 1, pp. 9–17, Jan. 2018.

[11] X. Zhang, Q. Miao, H. Zhang, and L. Wang, "A parameter-adaptive VMD method based on grasshopper optimization algorithm to analyze vibration signals from rotating machinery," *Mech. Syst. Signal Process.*, vol. 108, pp. 58–72, Aug. 2018.

[12] I. Aljarah, A. M. Al-Zoubi, H. Faris, M. A. Hassonah, S. Mirjalili, and H. Saadeh, "Simultaneous feature selection and support vector machine optimization using the grasshopper optimization algorithm," *Cognit. Comput.*, vol. 10, no. 3, pp. 478–495, Jun. 2018.

[13] M. Ebeed, S. Kamel, S. H. A. Aleem, and A. Y. Abdelaziz, "Optimal allocation of compensators," in *Electric Distribution Network Planning*. Springer, 2018, pp. 321–353.

[14] H. T. Ibrahim, W. J. Mazher, O. N. Ucan, and O. Bayat, "A grasshopper optimizer approach for feature selection and optimizing SVM parameters utilizing real biomedical data sets," *Neural Comput. Appl.*, vol. 31, no. 10, pp. 5965–5974, Oct. 2019.

[15] J. Luo, H. Chen, Q. Zhang, Y. Xu, H. Huang, and X. Zhao, "An improved grasshopper optimization algorithm with application to financial stress prediction," *Appl. Math. Model.*, vol. 64, pp. 654–668, Dec. 2018.

[16] S. Arora and P. Anand, "Chaotic grasshopper optimization algorithm for global optimization," *Neural Comput. Appl.*, vol. 31, no. 8, pp. 4385–4405, Aug. 2019.

[17] A. A. Ewees, M. A. Elaziz, and E. H. Houssein, "Improved grasshopper optimization algorithm using opposition-based learning," *Expert Syst. Appl.*, vol. 112, pp. 156–172, Dec. 2018.

[18] H. Liang, H. Jia, Z. Xing, J. Ma, and X. Peng, "Modified grasshopper algorithm-based multilevel thresholding for color image segmentation," *IEEE Access*, vol. 7, pp. 11258–11295, 2019.

[19] J. A. Momoh, M. E. El-Hawary, and R. Adapa, "A review of selected optimal power flow literature to 1993. II. Newton, linear programming and interior point methods," *IEEE Trans. Power Syst.*, vol. 14, no. 1, pp. 105–111, Feb. 1999.

[20] J. A. Momoh, R. Adapa, and M. E. El-Hawary, "A review of selected optimal power flow literature to 1993. I. nonlinear and quadratic programming approaches," *IEEE Trans. Power Syst.*, vol. 14, no. 1, pp. 96–104, Feb. 1999.

[21] R. C. Burchett, H. H. Happ, and D. R. Vierath, "Quadratically convergent optimal power flow," *IEEE Power Eng. Rev.*, vol. PER-4, no. 11, pp. 34–35, Nov. 1984.

[22] T. A. Al-Muhawesh and I. S. Qamber, "The established mega watt linear programming-based optimal power flow model applied to the real power 56-bus system in eastern province of Saudi Arabia," *Energy*, vol. 33, no. 1, pp. 12–21, Jan. 2008.

[23] H. Habibollahzadeh, G. X. Luo, and A. Semlyen, "Hydrothermal optimal power flow based on a combined linear and nonlinear programming methodology," *IEEE Power Eng. Rev.*, vol. 9, no. 5, pp. 51–52, May 1989.

[24] X. Yan and V. H. Quintana, "Improving an interior-point-based OPF by dynamic adjustments of step sizes and tolerances," *IEEE Trans. Power Syst.*, vol. 14, no. 2, pp. 709–717, May 1999.

[25] M. A. Abido, "Optimal power flow using particle swarm optimization," *Int. J. Elect. Power Energy Syst.*, vol. 24, no. 7, pp. 563–571, 2002.

[26] S. S. Reddy and C. S. Rathnam, "Optimal power flow using glowworm swarm optimization," *Int. J. Elect. Power Energy Syst.*, vol. 80, pp. 128–139, Sep. 2016.

[27] M. R. Adaryani and A. Karami, "Artificial bee colony algorithm for solving multi-objective optimal power flow problem," *Int. J. Electr. Power Energy Syst.*, vol. 53, pp. 219–230, Dec. 2013.

[28] M. A. Taher, S. Kamel, F. Jurado, and M. Ebeed, "Modified grasshopper optimization framework for optimal power flow solution," *Electr. Eng.*, vol. 101, no. 1, pp. 121–148, Apr. 2019.

[29] A. A. El-Fergany and H. M. Hasanien, "Single and multi-objective optimal power flow using grey wolf optimizer and differential evolution algorithms," *Electr. Power Compon. Syst.*, vol. 43, no. 13, pp. 1548–1559, Aug. 2015.

[30] M. Abdo, S. Kamel, M. Ebeed, J. Yu, and F. Jurado, "Solving non-smooth optimal power flow problems using a developed grey wolf optimizer," *Energies*, vol. 11, no. 7, p. 1692, 2018.

[31] T. Niknam, M. R. Narimani, M. Jabbari, and A. R. Malekpour, "A modified shuffle frog leaping algorithm for multi-objective optimal power flow," *Energy*, vol. 36, no. 11, pp. 6420–6432, Nov. 2011.

[32] M. A. Taher, S. Kamel, F. Jurado, and M. Ebeed, "An improved moth-flame optimization algorithm for solving optimal power flow problem," *Int. Trans. Electr. Energy Syst.*, vol. 29, no. 3, p. e2743, Mar. 2019.

[33] E. Barocio, J. Regalado, E. Cuevas, F. Uribe, P. Zúñiga, and P. J. R. Torres, "Modified bio-inspired optimisation algorithm with a centroid decision making approach for solving a multi-objective optimal power flow problem," *IET Gener., Transmiss. Distrib.*, vol. 11, no. 4, pp. 1012–1022, Mar. 2017.

[34] H. Pulluri, R. Naresh, and V. Sharma, "A solution network based on stud krill herd algorithm for optimal power flow problems," *Soft Comput.*, vol. 22, no. 1, pp. 159–176, Jan. 2018.
[35] H. R. E. H. Bouchekara, M. A. Abido, and M. Boucherma, "Optimal power flow using Teaching-Learning-Based optimization technique," *Electr. Power Syst. Res.*, vol. 114, pp. 49–59, Sep. 2014.
[36] N. Sinsuphan, U. Leeton, and T. Kulworawanichpong, "Optimal power flow solution using improved harmony search method," *Appl. Soft Comput.*, vol. 13, no. 5, pp. 2364–2374, May 2013.
[37] M. A. Abido, "Optimal power flow using tabu search algorithm," *Electr. Power Compon. Syst.*, vol. 30, no. 5, pp. 469–483, May 2002.
[38] M. Ghasemi, S. Ghavidel, M. M. Ghanbarian, H. R. Massrur, and M. Gharibzadeh, "Application of imperialist competitive algorithm with its modified techniques for multi-objective optimal power flow problem: A comparative study," *Inf. Sci.*, vol. 281, pp. 225–247, Oct. 2014.
[39] S. Duman, "Symbiotic organisms search algorithm for optimal power flow problem based on valve-point effect and prohibited zones," *Neural Comput. Appl.*, vol. 28, no. 11, pp. 3571–3585, Nov. 2017.
[40] M. A. Abido and N. A. Al-Ali, "Multi-objective optimal power flow using differential evolution," *Arabian J. Sci. Eng.*, vol. 37, no. 4, pp. 991–1005, Jun. 2012.
[41] M. S. Osman, M. A. Abo-Sinna, and A. A. Mousa, "A solution to the optimal power flow using genetic algorithm," *Appl. Math. Comput.*, vol. 155, no. 2, pp. 391–405, Aug. 2004.
[42] R. Gnanadass, P. Venkatesh, and N. P. Padhy, "Evolutionary programming based optimal power flow for units with non-smooth fuel cost functions," *Electr. Power Compon. Syst.*, vol. 33, no. 3, pp. 349–361, Dec. 2004.
[43] L. L. Lai, J. T. Ma, R. Yokoyama, and M. Zhao, "Improved genetic algorithms for optimal power flow under both normal and contingent operation states," *Int. J. Electr. Power Energy Syst.*, vol. 19, no. 5, pp. 287–292, Jun. 1997.
[44] H. R. E. H. Bouchekara, A. E. Chaib, M. A. Abido, and R. A. El-Sehiemy, "Optimal power flow using an improved colliding bodies optimization algorithm," *Appl. Soft Comput.*, vol. 42, pp. 119–131, May 2016.
[45] A. R. Bhowmik and A. K. Chakraborty, "Solution of optimal power flow using non dominated sorting multi objective opposition based gravitational search algorithm," *Int. J. Electr. Power Energy Syst.*, vol. 64, pp. 1237–1250, Jan. 2015.
[46] S. Duman, U. Güvenç, Y. Sönmez, and N. Yörükeren, "Optimal power flow using gravitational search algorithm," *Energy Convers. Manage.*, vol. 59, pp. 86–95, Jul. 2012.
[47] H. R. E. H. Bouchekara, "Optimal power flow using black-hole-based optimization approach," *Appl. Soft Comput.*, vol. 24, pp. 879–888, Nov. 2014.
[48] C. A. Roa-Sepulveda and B. J. Pavez-Lazo, "A solution to the optimal power flow using simulated annealing," *Int. J. Electr. Power Energy Syst.*, vol. 25, no. 1, pp. 47–57, Jan. 2003.
[49] K. Pandiarajan and C. K. Babulal, "Fuzzy harmony search algorithm based optimal power flow for power system security enhancement," *Int. J. Electr. Power Energy Syst.*, vol. 78, pp. 72–79, Jun. 2016.
[50] X. Yuan, P. Wang, Y. Yuan, Y. Huang, and X. Zhang, "A new quantum inspired chaotic artificial bee colony algorithm for optimal power flow problem," *Energy Convers. Manage.*, vol. 100, pp. 1–9, Aug. 2015.
[51] M. R. Narimani, R. Azizipanah-Abarghooee, B. Zoghdar-Moghadam-Shahrekohne, and K. Gholami, "A novel approach to multi-objective optimal power flow by a new hybrid optimization algorithm considering generator constraints and multi-fuel type," *Energy*, vol. 49, pp. 119–136, Jan. 2013.
[52] M. Ebeed, S. Kamel, and F. Jurado, "Optimal power flow using recent optimization techniques," in *Classical and Recent Aspects of Power System Optimization*. Amsterdam, The Netherlands: Elsevier, 2018, pp. 157–183.
[53] K. Ravi and M. Rajaram, "Optimal location of FACTS devices using improved particle swarm optimization," *Int. J. Electr. Power Energy Syst.*, vol. 49, pp. 333–338, Jul. 2013.
[54] S. M. Abd-Elazim and E. S. Ali, "Imperialist competitive algorithm for optimal STATCOM design in a multimachine power system," *Int. J. Electr. Power Energy Syst.*, vol. 76, pp. 136–146, Mar. 2016.
[55] S. Ranganathan, M. S. Kalavathi, C. A. Rajan C., "Self-adaptive firefly algorithm based multi-objectives for multi-type FACTS placement," *IET Gener., Transmiss. Distrib.*, vol. 10, no. 11, pp. 2576–2584, Aug. 2016.
[56] M. Ebeed, S. Kamel, and H. Youssef, "Optimal setting of STATCOM based on voltage stability improvement and power loss minimization using moth-flame algorithm," in *Proc. 18th Int. Middle East Power Syst. Conf. (MEPCON)*, Dec. 2016, pp. 815–820.
[57] H. Youssef, S. Kamel, and M. Ebeed, "Optimal power flow considering loading margin stability using lightning attachment optimization technique," in *Proc. 20th Int. Middle East Power Syst. Conf. (MEPCON)*, Dec. 2018, pp. 1053–1058.
[58] V. Tuzikova, J. Tlusty, and Z. Müller, "A novel power losses reduction method based on a particle swarm optimization algorithm using STATCOM," *Energies*, vol. 11, no. 10, p. 2851, 2018.
[59] S. Panda and N. P. Padhy, "Optimal location and controller design of STATCOM for power system stability improvement using PSO," *J. Franklin Inst.*, vol. 345, no. 2, pp. 166–181, Mar. 2008.
[60] S. M. A. Elazim and E. S. Ali, "Optimal SSSC design for damping power systems oscillations via gravitational search algorithm," *Int. J. Electr. Power Energy Syst.*, vol. 82, pp. 161–168, Nov. 2016.
[61] A. El-Zonkoly, "Optimal sizing of SSSC controllers to minimize transmission loss and a novel model of SSSC to study transient response," *Electr. Power Syst. Res.*, vol. 78, no. 11, pp. 1856–1864, Nov. 2008.
[62] S. Abd el-sattar, S. Kamel, and M. Ebeed, "Enhancing security of power systems including SSSC using moth-flame optimization algorithm," in *Proc. 18th Int. Middle East Power Syst. Conf. (MEPCON)*, Dec. 2016, pp. 797–802.
[63] S. Dutta, P. K. Roy, and D. Nandi, "Optimal allocation of static synchronous series compensator controllers using chemical reaction optimization for reactive power dispatch," *Int. J. Energy Optim. Eng.*, vol. 5, no. 3, pp. 43–62, Jul. 2016.
[64] I. Ngamroo and W. Kongprawechnon, "A robust controller design of SSSC for stabilization of frequency oscillations in interconnected power systems," *Electr. Power Syst. Res.*, vol. 67, no. 3, pp. 161–176, Dec. 2003.
[65] S. Panda, "Multi-objective evolutionary algorithm for SSSC-based controller design," *Electr. Power Syst. Res.*, vol. 79, no. 6, pp. 937–944, Jun. 2009.
[66] H. I. Shaheen, G. I. Rashed, and S. J. Cheng, "Optimal location and parameter setting of UPFC for enhancing power system security based on differential evolution algorithm," *Int. J. Electr. Power Energy Syst.*, vol. 33, no. 1, pp. 94–105, Jan. 2011.
[67] S. A. Taher and M. K. Amooshahi, "New approach for optimal UPFC placement using hybrid immune algorithm in electric power systems," *Int. J. Electr. Power Energy Syst.*, vol. 43, no. 1, pp. 899–909, Dec. 2012.
[68] H. C. Leung and T. S. Chung, "Optimal power flow with a versatile FACTS controller by genetic algorithm approach," in *Proc. IEEE Power Eng. Soc. Winter Meeting Conf.*, Jan. 2000, pp. 2806–2811.
[69] J. Sarker and S. K. Goswami, "Solution of multiple UPFC placement problems using gravitational search algorithm," *Int. J. Electr. Power Energy Syst.*, vol. 55, pp. 531–541, Feb. 2014.
[70] S. Dutta, P. K. Roy, and D. Nandi, "Optimal location of UPFC controller in transmission network using hybrid chemical reaction optimization algorithm," *Int. J. Electr. Power Energy Syst.*, vol. 64, pp. 194–211, Jan. 2015.
[71] B. V. Rao and G. V. N. Kumar, "Optimal power flow by BAT search algorithm for generation reallocation with unified power flow controller," *Int. J. Electr. Power Energy Syst.*, vol. 68, pp. 81–88, Jun. 2015.
[72] M. A. Taher, S. Kamel, F. Jurado, and M. Ebeed, "Optimal power flow solution incorporating a simplified UPFC model using lightning attachment procedure optimization," *Int. Trans. Electr. Energy Syst.*, vol. 30, no. 1, Jan. 2020, Art. no. e12170.
[73] *IEEE 30-Bus Test System Data*. [Online]. Available: https://labs.ece.uw.edu/pstca/pf30/pg_tca30bus.htm
[74] J. B. Hmida, T. Chambers, and J. Lee, "Solving constrained optimal power flow with renewables using hybrid modified imperialist competitive algorithm and sequential quadratic programming," *Electr. Power Syst. Res.*, vol. 177, Dec. 2019, Art. no. 105989.
[75] S. Verma and V. Mukherjee, "Firefly algorithm for congestion management in deregulated environment," *Eng. Sci. Technol., Int. J.*, vol. 19, no. 3, pp. 1254–1265, Sep. 2016.
[76] S. R. Paranjothi and K. Anburaja, "Optimal power flow using refined genetic algorithm," *Electr. Power Compon. Syst.*, vol. 30, no. 10, pp. 1055–1063, Oct. 2002.
[77] W. Ongsakul and T. Tantimaporn, "Optimal power flow by improved evolutionary programming," *Electr. Power Compon. Syst.*, vol. 34, no. 1, pp. 79–95, Jan. 2006.
[78] S. Sayah and K. Zehar, "Modified differential evolution algorithm for optimal power flow with non-smooth cost functions," *Energy Convers. Manage.*, vol. 49, no. 11, pp. 3036–3042, Nov. 2008.
[79] A.-A.-A. Mohamed, Y. S. Mohamed, A. A. M. El-Gaafary, and A. M. Hemeida, "Optimal power flow using moth swarm algorithm," *Electr. Power Syst. Res.*, vol. 142, pp. 190–206, Jan. 2017.

[80] M. Ghasemi, S. Ghavidel, M. Gitizadeh, and E. Akbari, "An improved teaching–learning-based optimization algorithm using Lévy mutation strategy for non-smooth optimal power flow," *Int. J. Electr. Power Energy Syst.*, vol. 65, pp. 375–384, Feb. 2015.

[81] U. Kiliç, "Backtracking search algorithm-based optimal power flow with valve point effect and prohibited zones," *Electr. Eng.*, vol. 97, no. 2, pp. 101–110, Jun. 2015.

[82] T. Niknam, M. R. Narimani, and R. Azizipanah-Abarghooee, "A new hybrid algorithm for optimal power flow considering prohibited zones and valve point effect," *Energy Convers. Manage.*, vol. 58, pp. 197–206, Jun. 2012.

[83] H. R. E. H. Bouchekara, A. E. Chaib, and M. A. Abido, "Optimal power flow using GA with a new multi-parent crossover considering: Prohibited zones, valve-point effect, multi-fuels and emission," *Electr. Eng.*, vol. 100, no. 1, pp. 151–165, Mar. 2018.

[84] H. Pulluri, R. Naresh, and V. Sharma, "A solution network based on stud krill herd algorithm for optimal power flow problems," *Soft Comput.*, vol. 22, no. 1, pp. 159–176, Jan. 2018.

[85] A. R. Kumar and L. Premalatha, "Optimal power flow for a deregulated power system using adaptive real coded biogeography-based optimization," *Int. J. Electr. Power Energy Syst.*, vol. 73, pp. 393–399, Dec. 2015.

[86] A. Shabanpour-Haghighi, A. R. Seifi, and T. Niknam, "A modified teaching–learning based optimization for multi-objective optimal power flow problem," *Energy Convers. Manage.*, vol. 77, pp. 597–607, Jan. 2014.

[87] J. Yuryevich and K. P. Wong, "Evolutionary programming based optimal power flow algorithm," *IEEE Trans. Power Syst.*, vol. 14, no. 4, pp. 1245–1250, Nov. 1999.

[88] H. Saadat, *Power System Analysis*. New York, NY, USA: McGraw-Hill, 1999.

[89] Z.-L. Gaing and R.-F. Chang, "Security-constrained optimal power flow by mixed-integer genetic algorithm with arithmetic operators," in *Proc. IEEE Power Eng. Soc. Gen. Meeting*, Jun. 2006, p. 8.

[90] *IEEE 57-Bus Test System Data*. [Online]. Available: https://labs.ece.uw.edu/pstca/pf57/pg_tca57bus.htm

AYMAN ALHEJJI received the B.S. degree in electrical power engineering from the Riyadh College of Technology, in 2007, the M.Sc. degree in engineering technology from Wayne State University, MI, USA, in 2010, and the Ph.D. degree in electrical and computer engineering from Southern Illinois University, Carbondale, IL, USA, in August 2014. Since October 2014, he has been as an Assistant Professor with the Department of Electrical and Electronics Engineering Technology, Yanbu Industrial College, Saudi Arabia. His research interests include adaptive and optimal control, and renewable energy power system modeling and control.

MOHAMED EBEED HUSSEIN received the B.S. degree from Aswan University, in 2005, the M.S. degree in electrical engineering from South Valley University, in 2013, and the jointly supervised Ph.D. degree from the Department of Electrical Engineering, Faculty of Engineering, Aswan University, Egypt, and the University of Jaen, Spain, in 2018. From 2008 to 2009, he was a Lecturer with the Aswan Technical Institute. From 2009 to 2017, he was a Maintenance Engineer at EFACO Company. He is currently an Assistant Professor with the Department of Electrical Engineering, Faculty of Engineering, Sohag University, Egypt.

SALAH KAMEL received the international Ph.D. degree from the University of Jaen, Spain (Main), and Aalborg University, Denmark (Host), in January 2014. He is currently an Assistant Professor with the Electrical Engineering Department, Aswan University. He is also the Leader of the Power Systems Research Group, Advanced Power Systems Research Laboratory (APSR Lab), Aswan, Egypt. He is also a Senior Research Fellow with the State Key Laboratory of Power Transmission Equipment and System Security and New Technology, School of Electrical Engineering, Chongqing University, Chongqing, China. His research activities include power system modeling, analysis and simulation, and applications of power electronics to power systems and power quality.

SAEED ALYAMI received the B.S. degree in electrical engineering from the King Fahd University of Petroleum and Minerals, Dhahran, Saudi Arabia, in 2004, and the M.S. and Ph.D. degrees in electrical and computer engineering from Wayne State University, Detroit, MI, USA, in 2010 and 2016, respectively. From 2004 to 2008, he was a Power Transmission Engineer with the Engineering and Design Department for Substations and Grid Integration, Saudi Electricity Company, Saudi Arabia. He is currently an Assistant Professor with Majmaah University. His research interests include smart grid, control of renewable energy systems, and distributed generation.